

Article

Unravelling the Antimicrobial, Antibiofilm, Suppressing Fibronectin Binding Protein A (*fnba*) and *cna* Virulence Genes, Anti-Inflammatory and Antioxidant Potential of Biosynthesized *Solanum lycopersicum* Silver Nanoparticles

Alsayed E. Mekky^{1,*}, Ahmed E. M. Abdelaziz², Fady Sayed Youssef³, Shymaa A. Elaskary⁴, Aly A. Shoun⁵, Eman A. Alwaleed⁶, Mahmoud Ali Gaber¹, Abdulaziz A. Al-Askar⁷, Alhadary M. Alsamman¹, Abdullah Yousef⁸, Gehad AbdElgayed⁹, Reda A. Suef¹, Mohamed A Selim¹, Ebrahim Saied¹ and Mohamed Khedr¹



Citation: Mekky, A.E.; Abdelaziz, A.E.M.; Youssef, F.S.; Elaskary, S.A.; Shoun, A.A.; Alwaleed, E.A.; Gaber, M.A.; Al-Askar, A.A.; Alsamman, A.M.; Yousef, A.; et al. Unravelling the Antimicrobial, Antibiofilm, Suppressing *Fibronectin Binding Protein A (fnba)* and *cna* Virulence Genes, Anti-Inflammatory and Antioxidant Potential of Biosynthesized *Solanum lycopersicum* Silver Nanoparticles. *Medicina* **2024**, *60*, 515. <https://doi.org/10.3390/medicina60030515>

Academic Editor: Amit K. Tripathi

Received: 6 February 2024

Revised: 1 March 2024

Accepted: 9 March 2024

Published: 21 March 2024

Correction Statement: This article has been republished with a minor change. The change does not affect the scientific content of the article and further details are available within the backmatter of the website version of this article.



Copyright: © 2024 by the authors. Licensee MDPI, Basel, Switzerland. This article is an open access article distributed under the terms and conditions of the Creative Commons Attribution (CC BY) license (<https://creativecommons.org/licenses/by/4.0/>).

- ¹ Botany and Microbiology Department, Faculty of Science, Al-Azhar University, Nasr City, Cairo 11884, Egypt; alsamman557@gmail.com (A.M.A.); redasuef@azhar.edu.eg (R.A.S.); mohamedselim@azhar.edu.eg (M.A.S.); hema_almassry2000@azhar.edu.eg (E.S.); mohamedkhedr.221@azhar.edu.eg (M.K.)
 - ² Botany and Microbiology Department, Faculty of Science, Port-Said University, 23 December Street, P.O. Box 42522, Port-Said 42522, Egypt; ahmed.abdelaziz@sci.psu.edu.eg
 - ³ Pharmacology Department, Faculty of Veterinary Medicine, Cairo University, Giza 12211, Egypt; fadyalsalhany@cu.edu.eg
 - ⁴ Medical Microbiology and Immunology Department, Faculty of Medicine, Menoufia University, Shihin El-Kom 32511, Egypt
 - ⁵ Microbiology and Immunology Department, Faculty of Pharmacy, El Salehey El Gadida University, El Saleheya El Gadida 44813, Egypt; aly.shoun@sgu.edu.eg
 - ⁶ Botany and Microbiology Department, Faculty of Science, South Valley University, Qena 83523, Egypt; eme_biologist@sci.svu.edu.eg
 - ⁷ Botany and Microbiology Department, Faculty of Science, King Saud University, P.O. Box 2455, Riyadh 11451, Saudi Arabia; aalaskara@ksu.edu.sa
 - ⁸ Basic & Medical Sciences Department, Faculty of Dentistry, Alryada University for Science & Technology, Sadat 32897, Egypt; abdullah.yousef@rst.edu.eg
 - ⁹ Integrated Molecular Plant Physiology Research, Department of Biology, University of Antwerp, 2020 Antwerp, Belgium; gehad.hegazygadabdelgayed@uantwerpen.be
- * Correspondence: alsayedessam@azhar.edu.eg

Abstract: *Background and Objectives:* Urinary tract infections [UTIs] are considered the third most known risk of infection in human health around the world. There is increasing appreciation for the pathogenicity of Gram-positive and Gram-negative strains in UTIs, aside from fungal infection, as they have numerous virulence factors. *Materials and Methods:* In this study, fifty urine samples were collected from patients suffering from UTI. Among the isolates of UTI microbes, six isolates were described as MDR isolates after an antibiotic susceptibility test carried out using ten different antibiotics. An alternative treatment for microbial elimination involved the use of biosynthesized silver nanoparticles (AgNPs) derived from *Solanum lycopersicum* [*S. cumini*]. *Results:* The sizes and shapes of AgNPs were characterized through TEM imaging, which showed spherical particles in a size range of 35–80 nm, of which the average size was 53 nm. Additionally, the silver nanoparticles (AgNPs) demonstrated inhibitory activity against *Staphylococcus aureus* (OR648079), exhibiting a 31 mm zone of inhibition at a minimum inhibitory concentration (MIC) of 4 mg/mL and a minimum bactericidal concentration (MBC) of 8 mg/mL. This was followed by *Aspergillus niger* (OR648075), which showed a 30 mm inhibition zone at an MIC of 16 mg/mL and a minimum fungicidal concentration (MFC) of 32 mg/mL. Then, *Enterococcus faecalis* (OR648078), *Klebsiella pneumoniae* (OR648081), and *Acinetobacter baumannii* (OR648080) each displayed a 29 mm zone of inhibition at an MIC of 8 mg/mL and an MBC of 16 mg/mL. The least inhibition was observed against *Candida auris* (OR648076), with a 25 mm inhibition zone at an MIC of 16 mg/mL and an MFC of 32 mg/mL. Furthermore, AgNPs at different concentrations removed DPPH and H₂O₂ at an IC₅₀ value of 13.54 µg/mL. Also, AgNPs at 3 mg/mL showed remarkable DNA fragmentation in all bacterial strains except *Enterococcus faecalis*. The phytochemical analysis showed the presence of different active organic components in the plant extract, which concluded that rutin was 88.3 mg/g, garlic acid was 70.4 mg/g, and tannic acid was

23.7 mg/g. Finally, AgNPs concentrations in the range of 3–6 mg/mL showed decreased expression of two of the fundamental genes necessary for biofilm formation within *Staphylococcus aureus*, *fmbA* (6 folds), and *Cna* (12.5 folds) when compared with the *RecA* gene, which decreased by one-fold when compared with the control sample. These two genes were submitted with NCBI accession numbers [OR682119] and [OR682118], respectively. **Conclusions:** The findings from this study indicate that biosynthesized AgNPs from *Solanum lycopersicum* exhibit promising antimicrobial and antioxidant properties against UTI pathogens, including strains resistant to multiple antibiotics. This suggests their potential as an effective alternative treatment for UTIs. Further research is warranted to fully understand the mechanisms of action and to explore the therapeutic applications of these nanoparticles in combating UTIs.

Keywords: antibiotic susceptibility; anti-inflammatory; antioxidant; pathogenicity; phytochemical analysis; urinary tract infections

1. Introduction

Urinary tract infection (UTI), or bacteriuria, is the medical term for the presence of bacteria in the urine. A clinical infection may begin with 10^5 bacteria/mL, but for epidemiological purposes, “notable” bacteriuria should be at least 10^5 bacteria/mL in freshly voided urine [1]. Urinary tract infections are the most globally common infectious disease, affecting over 10% of the world’s 150 million people daily. Uropathogenic *Escherichia coli* (UPEC) is consistently identified as the primary causative agent in both complicated and uncomplicated urinary tract infections [2]. Other specific microbes implicated in the pathogenesis of complicated UTIs include *Enterococcus* spp., *Klebsiella pneumoniae*, *Staphylococcus aureus*, *Pseudomonas aeruginosa*, and *Candida* spp. Similarly, the development of uncomplicated urinary tract infections is significantly impacted by pathogens, including *Klebsiella pneumoniae*, *Staphylococcus saprophyticus*, *Enterococcus faecalis*, Group B Streptococcus (GBS), *Proteus mirabilis*, *Pseudomonas aeruginosa*, *Staphylococcus aureus*, and *Candida* species. The fundamental mechanism underlying UTI pathogenesis involves the adherence of specific virulence factors present in the bacteria in the urethra. This process is followed by the colonization and subsequent ascension of the pathogen into the bladder through its appendages, such as flagella and pili. Once the pathogens attach to the bladder, complex interactions between the host and the pathogen occur, progressing the disease to more advanced stages [3]. The cluster of virulence factors is an important and remarkable cause of multidrug resistance in the urinary tract [4]. MDR bacteria in urine complicates empiric treatment of urinary tract infections and increases the prevalence of infection [5]. Globally, the extraordinary emergence and proliferation of multidrug-resistant bacterial infections pose a hazardous public health problem and are occurring in growing communities [6]. Recently, the emergence of the MDR uropathogen has led to an increase in nosocomial urinary tract infections worldwide [7]. Many microbial species and isolates have not yet been identified or described [8]. Due to the continuous increase in microbial multidrug resistance and the limitations of antibiotic therapy, there is an urgent need to develop effective antimicrobial agents with new mechanisms of action [9]. Researchers interested in generating nanoparticles are currently focusing on developing new strategies and materials to produce green nanomaterials [10,11]. Nanotechnology is a developing field of science focused on the fabrication of materials with nanosizes. The synthesis and application of nanomaterials have minimal impact on nature and provide maximum social benefits, as highlighted in this state of thinking [12]. Noble metal nanoparticles, including silver, gold, and titanium, have garnered significant interest for their potential use in biological applications because of their diverse therapeutic qualities. Silver nanoparticles (AgNPs), known for their low toxicity to mammalian cells and broad-spectrum antibacterial activity, are among the most extensively researched nanoscale particles [13]. More research reflects that nanosized silver particles exert a strong antibacterial effect due to their high specific surface

area [14]. Therefore, subsequent research has focused on nanoparticles as an alternative to conventional antimicrobial agents to control infections caused by multidrug-resistant bacteria (MDRB). Metal oxide nanoparticles have been shown to successfully function as promising antimicrobial agents against MDR isolates [15]. Essentially, many techniques, like mechanical, physical, and chemical, have been exploited to synthesize AgNPs. The biosynthesis approach, which makes use of microorganisms and plant extracts, has emerged as an environmentally benign synthetic method to overcome the drawbacks of physical and chemical methods [10,16]. Plant extracts provide an easy and advantageous way to create SNPs during biosynthesis since they are practical, easy to employ, rapid, affordable, and nontoxic. It is strongly advised to use plant extracts in order to produce AgNPs [17]. The outstanding antibacterial capabilities of plant materials can be attributed to their high content of secondary metabolites, such as enzymes, polysaccharides, alkaloids, tannins, phenols, terpenoids, and vitamins [18]. It is believed that the terpenoids and flavonoids found in the leaf extract aid in stabilizing the AgNPs [19]. Recently, there has been significant research into the biosynthesis of silver nanoparticles (AgNPs) using biological materials, such as plants and bacterial extracts as reducing agents, focusing particularly on their antibacterial activity. Nanomaterials are traditionally synthesized using one of two methods: i. “top-down” or ii. “bottom-up”. Using size reduction of bulk materials techniques, such as pulse wire discharge method, evaporation–condensation, ball milling, etc., the top–down approach produces nanoparticles. The bottom–up strategy involves the synthesis of nanoparticles (NPs) using chemical and biological mechanisms, wherein atoms self-assemble to form new nuclei that develop within tiny particles [20].

The common term “tomato”, *Solanum lycopersicum*, is chosen for this investigation. Its characteristics have led to the selection of this plant source. Tomatoes are a great source of several beneficial chemicals and antioxidants. They are staples in our daily diet. At the industrial level, tomatoes are used in large quantities to make purees and juices. *Solanum lycopersicum* has been shown to have antioxidant and anticancer properties. Certain phenolic chemicals are related to the function of an antioxidant. By lowering the body’s levels of free radicals, these substances guard against cell damage. The tomato plant was chosen for this study due to its nutritional characteristics and benefits [21].

AgNPs were produced by the oxidation of Ag^+ to Ag^0 by various biomolecules like flavonoids, carboxylic acids, phenolic acids, and aldehydes, along with proteins from plant extracts [22,23]. AgNPs are created through a simple, one-step process that does not produce toxic or expensive chemicals, making them safe, cheap, and environmentally friendly [24]. Recently, research has been intense on the biosynthesis of AgNPs with different shapes, molecular sizes, stability levels, and antibacterial efficacy in both plants and microorganisms [25]. In addition to being an effective material in reducing biofilm growth and preventing the spread of infectious diseases like nosocomial infections, urinary tract infections in children and adults are among the most common hospital-associated infections and are regarded as the third-most-known risk of infection regarding human health worldwide. AgNPs have been used laterally in medical clinics to reduce bacterial diseases [26]. Silver nanoparticles (AgNPs) have garnered significant attention, particularly in the field of biomedicine, due to their broad-spectrum and highly efficient antimicrobial and anticancer properties. Additionally, AgNPs have been explored for other biological activities, such as promoting bone healing and wound repair, enhancing the immunogenicity of vaccines, and exerting antidiabetic effects [27]. Understanding the biological mechanisms and potential cytotoxicity of AgNPs is crucial for optimizing their medical applications. The potential toxicity of AgNPs includes possible damage to various systems and organs in vivo, such as the skin, eyes, respiratory system, hepatobiliary system, central nervous system, urinary system, immune system, and reproductive system. One notable advantage of the proposed AgNPs over traditional silver-based antimicrobial agents is their enhanced efficacy at lower concentrations. The nanoscale size of AgNPs provides a larger surface area for interaction with microbial cells, thereby increasing their antimicrobial activity. Consequently, smaller amounts of AgNPs are needed to achieve the same antimicrobial

effect as larger quantities of bulk silver compounds. This lower concentration requirement can reduce the potential toxicity to human cells, making AgNPs a safer option for clinical applications. Furthermore, the increased efficacy at lower concentrations can result in cost savings in both the manufacturing and application of AgNP-based products [28–30].

Recently, bacterial biofilms have been recognized as a public health concern. They are crucial to the survival of dangerous bacteria, which makes them increasingly resistant to medications [31]. So, AgNPs were also in competition with biofilm formation [32]. Our novelty in this research is to study the antimicrobial, antioxidant, and anti-inflammatory activity of tomato-leaf extract in comparison with green biosynthesized AgNPs and their effect on the expression of two fundamental genes of biofilm formation in *Staphylococcus aureus* at concentrations below its MIC.

2. Materials and Methods

2.1. Collection of Plant Material and Chemicals

Solanum lycopersicum leaves were collected from El-Qalubya Government, Cairo, Egypt, (GPS, N: 30°11'39.34", E: 31°26'1.23"). The chemicals and reagents, silver nitrate (AgNO₃), dimethyl sulfoxide (DMSO), 2,2-diphenyl-1-picrylhydrazyl (DPPH), Tryptic Soy Broth (TSB), nutrient broth, agar, potato dextrose agar [PDA], purple p-iodonitrotetrazolium (INT, 0.2 mg/mL), NaOH, aluminum chloride, H₂SO₄, HCL, alcoholic KOH, MgCl₂, methanol, ascorbic acid (Vitamin C), sodium phosphate buffer, and NaCl were of AR grade and procured from Sigma-Aldrich, Cairo, Egypt). All biological syntheses in the current study were achieved using distilled water (dis. H₂O).

2.2. Preparation of Plant Extract and Biosynthesis of AgNPs

The tomato leaves were hand-pulled after being baked until completely dry. To prepare the extract, 50 g of powdered dry leaves were suspended in a solution of 50 mL of MeOH and 50 mL of H₂O. The combination was then sonicated, and the mixture was filtered using Whatman filter paper no. 1. The residual water was removed through freeze-drying and stored at 4 °C, while the methanol was subsequently evaporated using a rotary [33]. The protocol of Oves et al. [34] was followed with some modifications. One mM of a 50 mL aq AgNO₃ solution is frequently added to 5 mL of tomato-leaf extract in a 250 mL conical flask with vigorous agitation at 90 °C for 60 min in order to synthesize biogenic silver nanoparticles. A change in the mixture's color served as our observation for the formation of AgNPs. The color of the silver nitrate solution changed to brownish yellow within 5 min, indicating that the bioreduction of the silver ions was rapid, confirming the preparation of AgNPs. Biosynthesized AgNPs were purified by centrifugation at 10,000 rpm for 10 min and were washed three times with DW to remove loosely attached biomolecules. Then AgNPs were transferred into a clean bottle in a dark place for further studies.

2.3. AgNPs Characterization

Different techniques were used to characterize biosynthesized silver nanoparticles. The change in color of the reaction mixture, following the reduction of Ag⁺ to Ag⁰ nanoparticles (NPs) by an extract derived from *S. cumin* leaves, was confirmed or assessed through a visual examination. UV light's optical absorption characteristics were ascertained using a JASCOVIS-730 dual-beam spectrometer. The absorption spectrum was collected between 200 and 700 nm, with an additional wavelength increase of around 0.2 nm. The transmission electron microscope (EOL MODEL 1200EX, Ltd., Tokyo, Japan), running at 120 kV, was used to evaluate the micrographs of the samples. For this purpose, a drop of NPs solution was added to a carbon-coated copper grid and left to dry before being placed on a specimen holder. X-ray diffraction (XRD) characterization was conducted using a powder diffractometer (Ultima IV, Rigaku, Japan) equipped with a copper target, generating K α 1 radiation at a wavelength of 1.54060 Å. The 2 θ range, which spans from 10 to 80 degrees, was measured. The 2 θ / θ continuous mode was used for X-ray scanning, with a step size of 0.02 and a scanning rate of 2 degrees per minute. Both the voltage and the current in

the tubes stay constant at 40 kilovolts (kV) and 40 milliamperes (mA). The average Ag-NP sizes were measured using the Debye–Scherrer equation [35] as follows:

$$D = K\lambda/\beta\cos\theta$$

Here, D is the average particle size, K is the Scherrer constant (0.9), λ is the wavelength of X-ray radiation (0.154 nm), and β and θ are the half of maximum intensity and Bragg's angle, respectively.

Fourier transform infrared spectroscopy (FT-IR) measurements were conducted using FTIR spectrometer (JASCO-6700, Tokyo, Japan), covering the spectral range from 400 to 4000 cm^{-1} . An aliquot of 300 μL of Ag-NPs, which was mixed with potassium bromide (10 mg), was oven-dried.

2.4. Molecular Identification of MDR Bacterial Isolates

During the period from January 2021 to August 2021, isolates were obtained from urine samples of fifty patients (20 male and 30 female) who were hospitalized at Menoufia University hospitals with UTIs and significant bacteriuria. In accordance with the Declaration of Helsinki, the study received approval from the Ethical Committee of Human Rights of Research at Menoufia University (12/2023MICR4-2). Each participant in this study signed a written informed consent form after being informed about it. All data are stored and maintained. The clinical specimens were streaked on CLED agar plates as soon as they were brought to the Medical Microbiology and Immunology Department's laboratory. Significantly positive isolates were purified and identified after a 24 h incubation period [36]. Using the Genomic Wizard DNA kit (Promega, Madison, WI, USA), whole bacterial genomic DNA was extracted from all the tested isolates in accordance with the manufacturer's instructions. The 16S rDNA gene was amplified using two widely used bacterial primers: the RW primer (CCAGCCGCAGGTTCCCCT) and the 16Sb FW primer (CCGTGGCGGCAGGCTTAACA) [37]. The following were the PCR conditions: 35 cycles total—94 °C/30 s for the denaturation step, 55 °C/60 s for the annealing step, 72 °C/90 s for the extension step, and 72 °C/180 s for the final extension step.

The exact dimensions of the amplified PCR product, a fragment of approximately 1500 base pairs, were confirmed by electrophoresis of 10-microliter aliquots on a 1% agarose gel containing 0.5 micrograms per milliliter of ethidium bromide. The gels were inspected and captured on camera using a UV lamp [38]. Next, amplicons were cleaned using a QIAquick spin column (Chatsworth, CA-based Qiagen Inc. (San Diego, CA, USA)). As previously stated, ten purified amplicons were sequenced using a Perkin Elmer 377 DNA sequencer in conjunction with a Dye Deoxy Terminator Cycle Sequencing Kit (Perkin Elmer, Foster City, CA, USA).

2.5. DNA Fragmentation Induced by AgNPs MIC

AgNPs were applied at MIC to two isolated bacterial cells to examine DNA fragmentation. The procedure for isolating DNA is shown in the manufacturer's brochures (Thermo Fisher Scientific, Santa Clara, CA, USA). A DNA purification kit was utilized. After quantification, 4 μg of each DNA sample were electrophoresed on a 1.6% agarose gel that was UV-irradiated and treated with 5 $\mu\text{g}/\text{mL}$ ethidium bromide [39].

2.6. Minimum Inhibitory Concentration (MIC) and Minimum Bactericidal Concentration (MBC)

The individual strains were cultured in Tryptic Soy Broth (TSB) overnight until they reached an optical density at 595 nm (OD₅₉₅) of 1. Subculture 1 was 1000 in (TSB). One hundred microliters of bacterial culture were sampled, followed by the addition of 10 microliters of an appropriate serial dilution of AgNPs (NPs/mL) to 96-well plates (F-bottom, Sterilin). The optical density (OD₅₉₅) was measured using a spectrophotometer called "SPECTRONIC GENESYSTEM 2PC", manufactured by Spectronic, Melville, NY, USA, during a 24 h incubation period at 37 °C.

Forty milliliters of purple p-iodo-nitrotetrazolium (INT, 0.2 mg/mL, Sigma-Aldrich) were added to the microplate wells, and the plates were incubated for an additional 30 min at 37 °C to verify the inhibition of bacterial growth through the lack of metabolic activity [40]. As previously mentioned by Feizi et al. [41], the MIC for the INT assay was found to be the NP concentration that stopped the least amount of color change. Growth was determined by measuring the difference between the OD595 reading and the negative control, Trypticase soy agar (TSA alone), at least two times.

After that, MBC tests were conducted. A 99.9% CFU (3 log) rise in the initial inoculum over the course of a 24 h incubation period was considered bactericidal effectiveness. Fifty ccs from each well of the MIC plate were transferred to a fresh, sterile (TSA) plate, and the MBC was calculated overnight. After a day at 37 °C, viable colonies were counted. This test has a detection limit of 10¹ CFU/mL.

Using agar well diffusion, the antifungal activity of AgNPs was assessed against *Candida auris* (OR648076) and *Aspergillus niger* (OR648075). Every fungal strain that was evaluated was cultivated on PDA plates and kept at 30 °C for a duration of 3–5 days [42]. After the preparation of the fungal suspension in a sterile phosphate buffer solution (PBS), with pH 7.0, the inoculum was adjusted to 10⁷ spores/mL using a cell-counter chamber. Agar MEA plates were evenly filled with one milliliter. The wells (9 mm) were cut using a sterile cork borer. One hundred µL of AgNPs and AgNO₃ were then added to each well separately, and the mixture was allowed for two hours at 4 °C. Following the application of a conventional antifungal, chloramphenicol, the plates were incubated at 30 °C for three days. The inhibitory zones were identified and noted following incubation. Additionally, several Ag NP concentrations were assessed for their antifungal properties in order to determine the minimal fungus concentration (MFC).

2.7. Antioxidant Activity of the Synthesized AgNPs

A method for measuring antioxidant activity is the DPPH radical-scavenging technique. One method of evaluating the capacity of different plant-leaf extracts to scavenge free radicals is to utilize 1,1-diphenyl-2-picryl hydrazyl (DPPH). In short, an ethanol-based 0.1 mM DPPH solution was prepared. One milliliter of this solution was combined with three milliliters of different extracts in ethanol at different concentrations (3.9, 7.8, 15.62, 31.25, 62.5, 125, 250, 500, and 1000 µg/mL). Here, only extracts that dissolve in ethanol are utilized, and the different strengths of the extracts were made using the dilution process. The mixture was well-shaken and then allowed to stand at room temperature for 30 min. The absorbance was then measured with a UV–VIS Milton Roy spectrophotometer at 517 nm. As the reference-standard compound, ascorbic acid was used in an experiment [43].

$$\% \text{ inhibition or DPPH scavenging action} = A_0 - A_1 / A_0 \times 100.$$

where A1 represented the absorbance while the test or standard sample was present, and A0 represented the absorbance of the control response.

2.8. Anti-Inflammatory Effects of AgNPs

2.8.1. Preparation of Erythrocyte Suspension

Three milliliters of freshly drawn blood from healthy participants were centrifuged into heparinized tubes for ten minutes at 3000 rpm. The red-blood-cell pellets were dissolved in a supernatant equivalent to normal saline, quantified, and then reconstituted as a 40% v/v suspension using an isotonic buffer solution (10 mM sodium phosphate buffer consisting of 0.2 g NaH₂PO₄, 1.15 g Na₂HPO₄, and 9 g NaCl in 1 L of distilled water). The final pH was adjusted to 7.4 [44].

2.8.2. Hypotonicity-Induced Hemolysis

Distilled water was used to dissolve the extract samples for this test, creating a hypotonic solution. Graded extract dosages (100, 200, 400, 600, 800, and 1000 µg/mL) were

added to pairs of double centrifuge tubes (per dose) in the hypotonic solution (5 mL). In addition, pairs of double centrifuge tubes were filled with an isotonic solution (5 mL) containing graded doses of extract (100–1000 µg/mL) (per dose). Five milliliters each of indomethacin 200 µg/mL and distilled water, the excipient, were found in the control tubes. Each tube should contain 0.1 milliliter of red-blood-cell suspension. Gently stir. After 1 h of room-temperature (37 °C) incubation, the mixture was centrifuged for three min at 1300× *g*. Using a spectrophotometer (Milton Roy), the absorbance (OD) of the hemoglobin that makes up the supernatant was measured at 540 nm. The hemolysis ratio was calculated with the assumption that, in the event of distilled water, the resulting hemolysis amount would be 100%. The extract's hemolysis inhibition ratio was determined [44].

$$\% \text{ Hemolysis inhibition} = 1 - ((\text{OD2} - \text{OD1}) / (\text{OD3} - \text{OD1})) \times 100$$

where OD1 is the test sample's absorbance in an isotonic solution.

OD2 is the test sample's absorbance in a hypotonic solution.

OD3 is the control sample's absorbance in a hypotonic solution.

2.9. Phytochemical Analysis

A phytochemical analysis is usually confirmed to evaluate either the presence (positive [+]) or absence (negative [−]) of certain chemicals within plant crude extract. Molisch's test for the presence of carbohydrates is noted by Sofowora [45]. A froth test is used for saponins, according to Mojab et al. [46]. A ferric chloride test is used for tannins, according to Trease and Evans [47]. A biuret test is used for proteins besides amino acids which is described according to Salna et al. [48]. A lead acetate test, a NaOH test, an aluminum chloride test, and a H₂SO₄ test for flavonoids according to [23,24]. A ferric chloride test is used for phenols, according to Preshant et al. [49]. A glycosides test and Borntrager's test is for glycosides, according to Treare and Evans [47] and Harsha et al. [50]. The Keller–Kiliani test and Legal's test are for cardiac glycosides, according to Balbaa [51] and Preshant et al. [49]. Borntrager's test (for free anthracene derivatives) and a modified Borntrager's test (for combined anthracene derivatives) are for anthraquinone, according to Sofowora [45], and Trease and Evans [47]. Wagner's test, Dragendroff's test, and Hager's test are for alkaloids, according to [52,53]. An HCl test is for phlobatannins, according to Abdullahi et al. [54]. An alcoholic KOH test and a Ninhydrin test are for quinone, according to Egbuna et al. [55] and Kebede et al. [56]. The test for resins is conducted according to the method described by Egbuna et al. [55].

Investigation of Total Active Materials

The total phenolic content (TPC) of the sample was determined using the Folin–Ciocalteu method, as documented by Makkar [57]. Using the aluminum chloride method, the total flavonoid content (TFC) of our plant extract was also determined [58]. The Folin–Ciocalteu method was used to identify and assess the total tannins in the sample [59]. The proportion of saponin content was determined using the methods of Lim et al. [60]. At last, the total alkaloids were assessed using the methodology of Herborne [61], which had been validated.

2.10. Static Biofilm Assay

With minor modifications, static biofilms were produced in microtiter plates utilizing the crystal violet staining technique, essentially as previously reported by Saber et al. [62]. Individual strains were grown compactly on TSA plates for a whole night. They were then suspended in TSB and adjusted to an OD₅₉₅ of 0.02. A 96-well microtiter plate (U-bottom, Sterilin) containing approximately 130 µL of this dilution was incubated for 24 h at 37 °C. Ten µL of AgNP colloidal solution containing 10⁵ NP/mL were added after a 24 h period. As controls, 10 µL of two aqueous plant extracts were added. To evaluate the amount of biofilm, biofilms were dissolved in 96% ethanol and stained with 0.1% crystal violet, and their OD₅₉₅ was quantified using an Infinite_F50 robotic microplate reader (ostrich).

2.11. Ribonucleic Acid Isolation and Complementary Deoxyribonucleic Acid Synthesis

2.11.1. Ribonucleic Acid Isolation

Total ribonucleic acids (RNAs) were extracted from the 72 h fermentation of the *S. aureus* strain, which was cultivated in a liquid nutrient broth medium, through Trizol (Gibcol), according to the manufacturer's protocol. cDNA for the sense strand was synthesized via the Advantage RT-PCR Kit (Clontech, Alo Alto, CA, USA).

2.11.2. Conventional Reverse Transcription Polymerase Chain Reaction Amplification

Fifty μ L reactions of polymerase chain reactions PCR were conducted with primers in Table 1 for the *fnbA* gene within *S. aureus* and Table 2 for the amplification of the *Cna* gene for the same strain. These primers were created using the NCBI site's Primer BLAST tool. The reference housekeeping gene is *RecA* which also amplified through specific primers listed in Table 3. The PCR reaction mixture consists of 120 ng of synthesized cDNA, 195 mM dNTPs, 0.1 mM of each primer, 1.7 mM Mg Cl₂, one unit of Taq DNA polymerase (Takara, Tokyo, Japan), and sterile water to adjust the volume to 50 μ L. The following describes the PCR program.

Table 1. Specific primers used to detect the *fnbA* gene in the *S. aureus* strain.

Primer	Sequence (5'->3')	Tm	GC%	Self 3' Complementarity	References
Forward primer-1	AGCGGTAACCAGTCATTCGAG	60	52	2.0	This study
Reverse primer-1	TTGGCGGCGTTGTATCTTCT	60	50	0	This study
Forward primer-2	GAAGATACAACGCCGCAAC	59.9	55	0	This study
Reverse primer-2	AGGTTCTCTTTTGC GG TG	58.8	50	0	This study

Table 2. Specific primers used to detect the *Cna* gene in the *S. aureus* strain.

Primer	Sequence (5'->3')	Tm	GC%	Self 3' Complementarity	References
Forward primer-3	AAGGTGAACAGGTGGGTCAA	59.08	50	0	This study
Reverse primer-3	CACTACTGTGCCCGCTTCA	57.84	50	1	This study

Table 3. Specific primers used to detect the *RecA* gene in the *S. aureus* strain.

Primers	Sequence (5'->3')	Tm	GC%	Self 3' Complementarity	References
FW 1RecA	GCCCTAATTGGTCCAGGCG	45	44.3	0	[63]
RW 1 RecA	ACAACGGCGTTCTCTCCTAT	45	44.4	0	[63]
FW 2 RecA	ACACAACGTCATTGCAAATGTGA	45	44.3	1.0	[63]
RW 2 RecA	GCCTGGACCAATTAGGGCAT	45	44.3	1.0	[63]

After four minutes of denaturation at 93 °C, there were 29 cycles of 35 s at 93 °C, 45 s at 50 °C, one minute at 45 °C, and a final 6 min extension at 72 °C. A %TAE buffer, which has 1 mM Na-acetic acid (EDTA) and 40 mM Tris-Acetate at pH 7.6, was used to separate the agarose gel. Gels were examined under a UV lamp after electrophoresis and stained with ethidium bromide (0.5 mg/mL). The size was determined using a standard-length DNA ladder (GeneRuler™ 100 bp DNA Ladder, MBI Fermentans, Vilnius, Lithuania).

2.11.3. Real-Time PCR Amplification Conditions

Using the primers listed in Tables 1 and 2, complementary DNA (cDNA) from the *S. aureus* strain was subjected to semiquantitative PCR. The PCR mixture consisted of 12.5 μ L of 2 \times Quantitech SYBR® Green RT Mix (Fermentase.com), 1 μ L of 25 pm/L forward and reverse primers, 1 μ L of 50 ng cDNA, and 9.25 μ L of RNase-free water. Two primers specific for the *fnbA* gene were found in Table 1, while the two primers specific for *Cna* were found in Table 2. The initial denaturation step in PCR real-time programs lasts for

ten minutes at 93 °C for 40 cycles of 15 s. Annealing for 35 s at 45 °C and extending for 30 s at 72 °C.

2.11.4. Data Analysis

Using the dd Δ ct technique and Microsoft Excel 2016, a comparative quantification analysis was carried out.

2.12. Statistical Analysis

To ascertain the major variations based on many growth characteristics, the data were statistically evaluated. A one-way analysis of variance test utilizing the statistical ANOVA program Spss v17, was used to examine the variables for differences between the various concentrations of the biosynthesized silver nanoparticles caused by variations in the exposure period.

3. Results

3.1. Green Synthesis of AgNPs

Tomato-leaf extract was utilized as a reducing agent for the silver nitrate solution during the biosynthesis process. By changing the color of silver nitrate from clear to yellow or deep brown, the creation of NPs was detected (Figure 1).

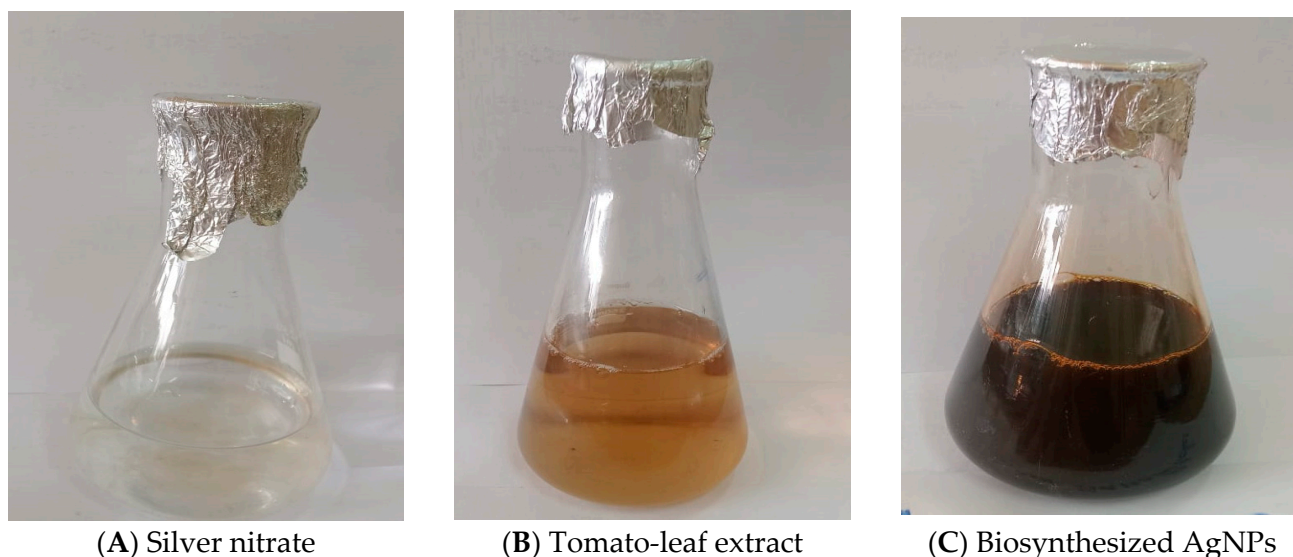


Figure 1. AgNPs were biosynthesized through tomato-leaf extract. Where (A) is silver nitrate soln; (B) is tomato-leaf extract and (C) is the biosynthesized AgNPs.

3.2. Characterization of AgNPs

3.2.1. UV–Vis Spectrophotometry

AgNPs were characterized by topographical surveys and a physiochemical investigation. Figure 2 shows the UV–visible spectra of AgNPs. The first indication of AgNP production in the UV–Vis spectrophotometer investigation was a color shift to deep brown. Color changes may be attributed to the excitation of the surface plasmon resonance of the produced nanoparticles [64]. With a distinctive peak at 457 nm, surface plasmon resonance SPR provided additional confirmation that Ag had been reduced to AgNPs. The predicted value falls inside the range that was previously mentioned [65–67].

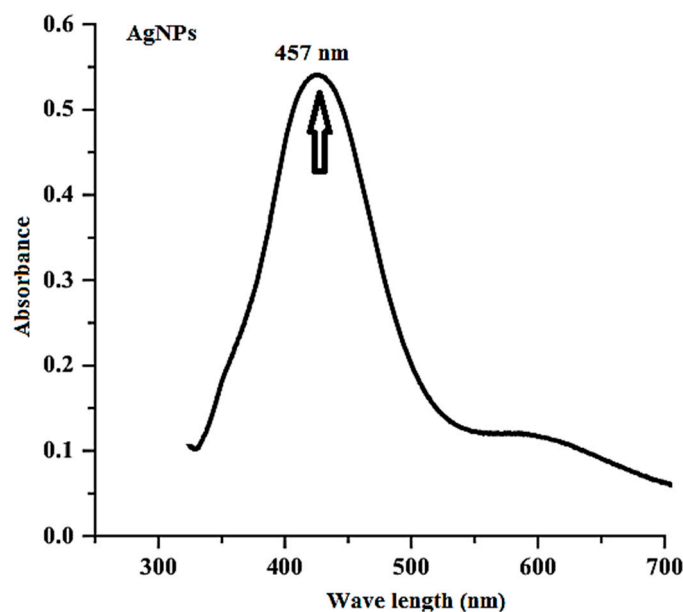


Figure 2. Surface plasmon resonance of biosynthesized AgNPs by using *Solanum lycopersicum*.

3.2.2. XRD Analysis

Biosynthesized NP crystallinity was examined through XRD. Characteristic peaks were determined at 2θ values of 31.7° , 45.6° , 56.3° , and 75.2° , corresponding to the planes (111), (200), (220), and (311). Figure 3A confirms the AgNPs have a face-centered cubic structure. Furthermore, using Debye–Scherrer equation, the crystallite size mean of the synthesized NPs was found to be 55 nm.

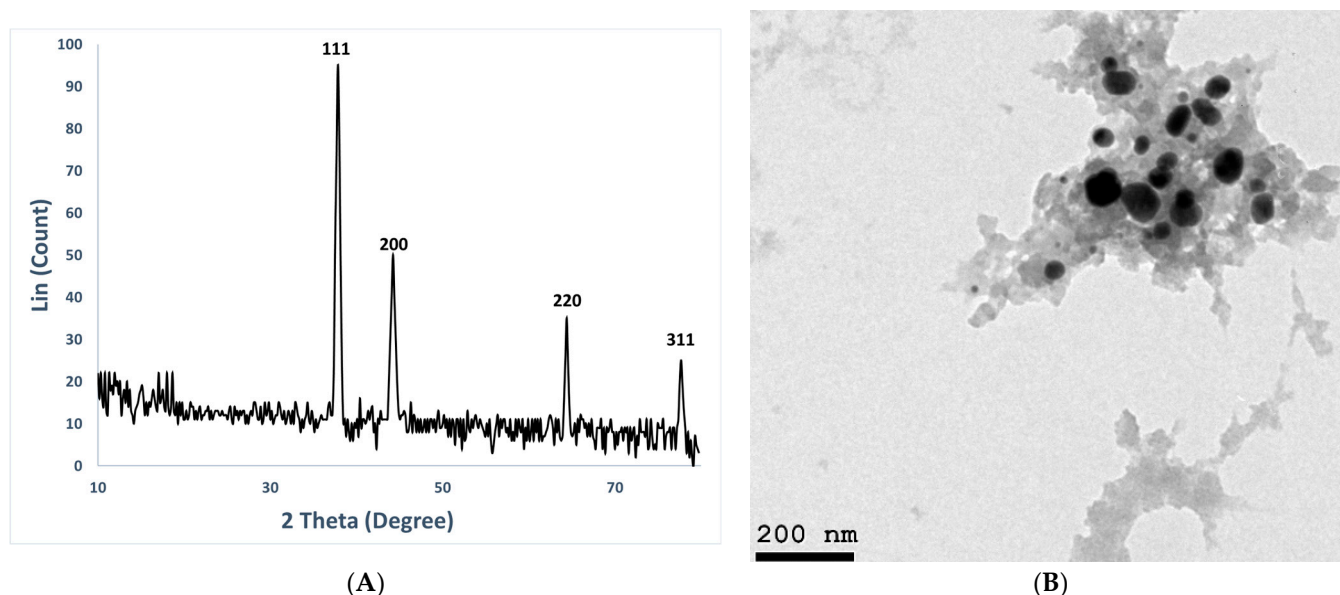


Figure 3. (A) XRD analysis and (B) TEM imaging of biosynthesized AgNPs.

3.2.3. TEM Characterization of Biosynthesized AgNPs

AgNPs were created, and their shape and size were characterized using TEM examination. TEM micrographs (Figure 3B) showed that the particles were almost spherical in shape and monodispersely distributed with little agglomeration. The presence of biomolecules and other metabolites in biomass filtrate, which are utilized in the bioreduction and bio-capping of produced nanoparticles, may be the cause of the variation in nanosize and nanoshape [68]. The AgNPs are evenly distributed and do not aggregate, as seen by the

TEM picture. The diameters of the nanoparticles varied from 35 to 80 nm, with an average size of 53 nm.

3.2.4. Fourier Transform Infrared (FT-IR) Spectroscopy

To determine the potential biomolecules in charge of the reduction of Ag^+ ions and capping of the bioreduced silver nanoparticles produced by *Solanum lycopersicum* [*S. cumini*] leaf extracts, FT-IR studies were performed. The FT-IR spectra of the nanoparticles produced are shown in Figure 4. The various functional groups were seen in the FT-IR peaks. Data represented in Figure 4 revealed intense absorption peaks at 3348, 2966, 2154, 1586, 1374, 1045, 822, 644, 531, 440, and 410 cm^{-1} .

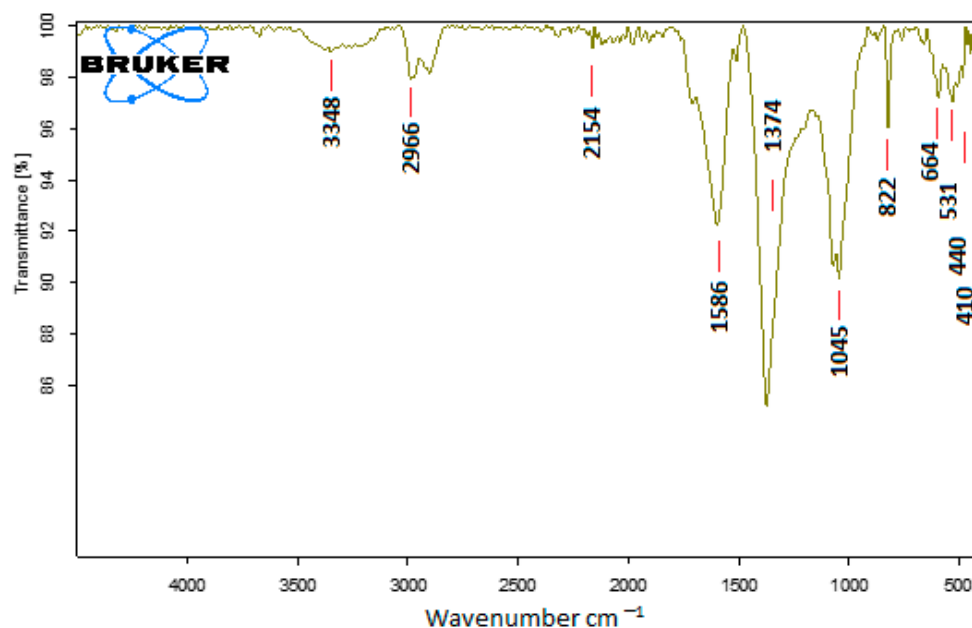


Figure 4. FTIR analysis of biosynthesized AgNPs by using *Solanum lycopersicum*.

3.3. Molecular Identification of MDR Isolates

Sequencing of the PCR products of the tested MDR bacterial and fungal strains revealed that *Staphylococcus aureus* (OR648079), *Enterococcus faecalis* (OR648078), *Acinetobacter baumannii* (OR648080), *Klebsiella pneumonia* (OR648081), *Aspergillus niger* (OR648075), and *Candida auris* (OR648076). These phylogenetic trees were built using Mega 11 in comparison to the NCBI BLAST sequences that were the most comparable (Figures 5 and 6).

3.4. DNA Fragmentation

In our attempt to explain the mechanism by which AgNPs eliminate microbial growth, we used concentrations of AgNPs lower than MIC, MBC, and MFC in order to study their effect on DNA. The findings reported that 3 mg/mL was the best AgNPs concentration, resulting in DNA fragmentation in three bacterial tested strains among four. DNA fragmentation was not noted with *Enterococcus faecalis* alone (Figure 7). Adeyemi et al. [69] noted that DNA damage was induced by AgNPs in addition to oxidative stress. AgNPs cause DNA fragmentation in bacteria, which finally results in cellular death [70].

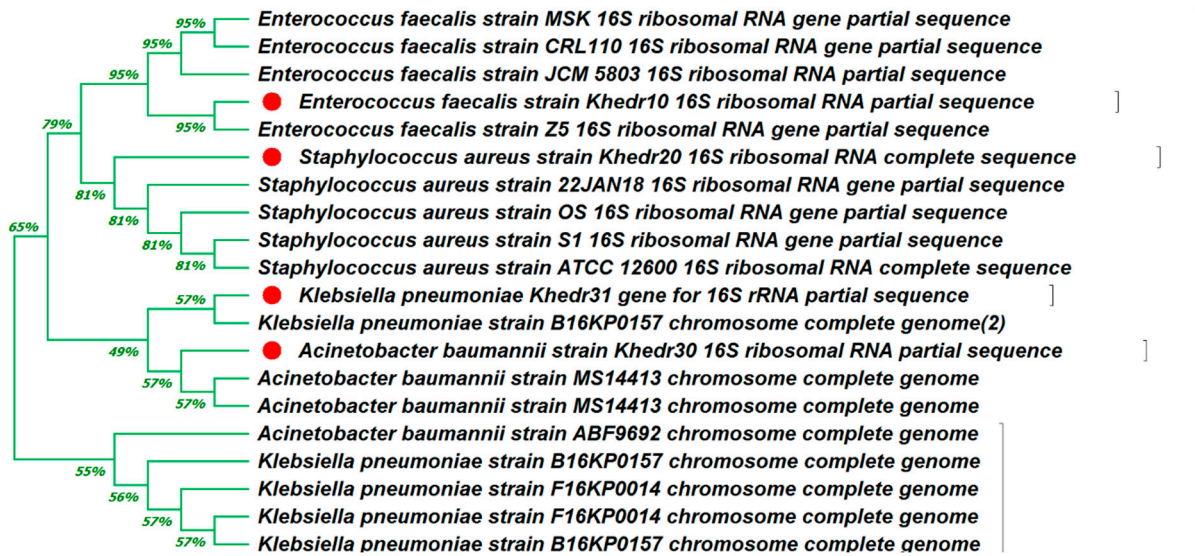


Figure 5. Phylogenetic tree of 16S rDNA-based identification of four MDR bacterial test strains (*Staphylococcus aureus* (OR648079), *Enterococcus faecalis* (OR648078), *Acinetobacter baumannii* (OR648080), and *Klebsiella pneumonia* (OR648081)) through Mega 11 software (version 11.0.13). The genetically defined organisms are marked with a red circle.

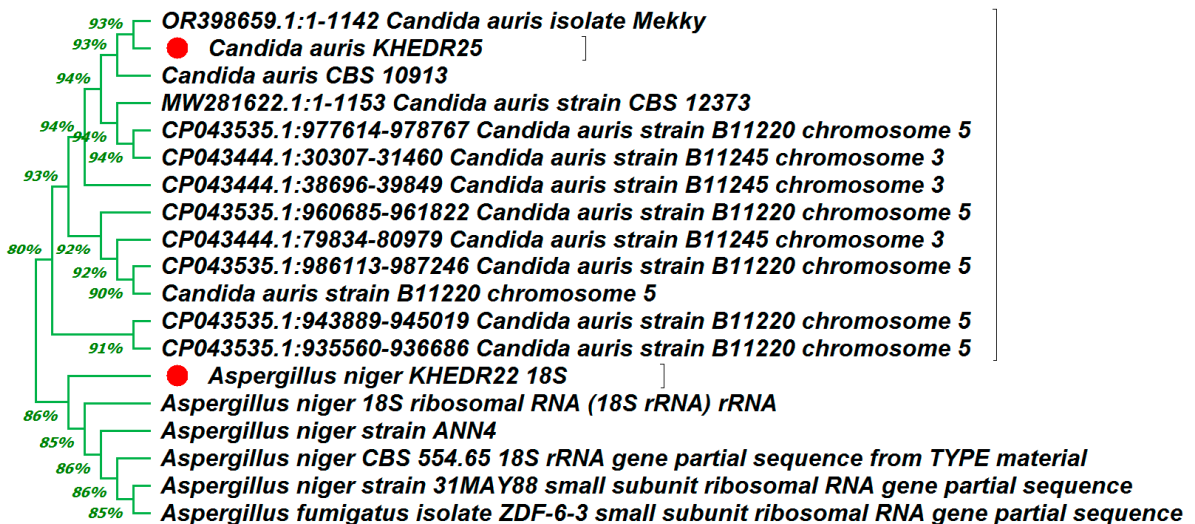


Figure 6. Phylogenetic tree of 18S rDNA-based identification of two MDR fungal test strains (*Aspergillus niger* (OR648075), and *Candida auris* (OR648076)) through Mega 11 software. The genetically defined organisms are marked with a red circle.

3.5. Antioxidant Assays

Using DPPH and H₂O₂ models, the antioxidant capacities of the tomato-leaf extract in an aqueous solution, AgNPs, and standards were investigated. Using ascorbic acid as a reference, the DPPH elimination activity of the studied materials is displayed in Table 1. AgNPs eliminated DPPH significantly in amounts of 92.5, 85.5, 78.7, 71.7, 64.7, 57.8, 51.1, 44.4, 38.1, and 31.4%, which corresponded to an average (IC₅₀ value of 13.54 µg/mL) at various doses (1000, 500, 250, 125, 62.5, 31.25, 15.625, 7.8125, 3.9, and 1.95 µg/mL). These activities, however, paled in comparison to ascorbic acid's (IC₅₀ 3.45 µg/mL). With an IC₅₀ value of 27, the crude plant extract showed a greater inhibitory impact than Ag NP but a lower one than ascorbic acid at the same dosages (Figure 8 and Table 4).

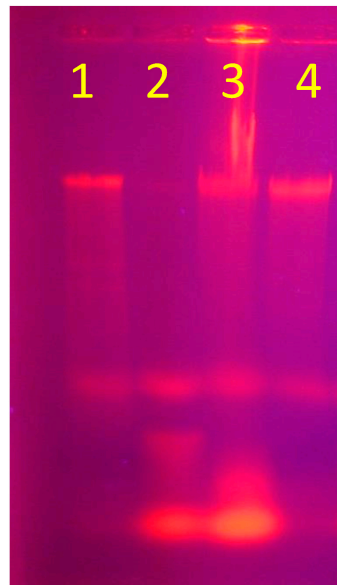


Figure 7. DNA fragmentation of four tested bacterial strains: band 1: *Acinetobacter baumannii*, band 2: *Enterococcus faecalis*, band 3: *Staphylococcus aureus*, and band 4: *Klebsiella pneumonia*.

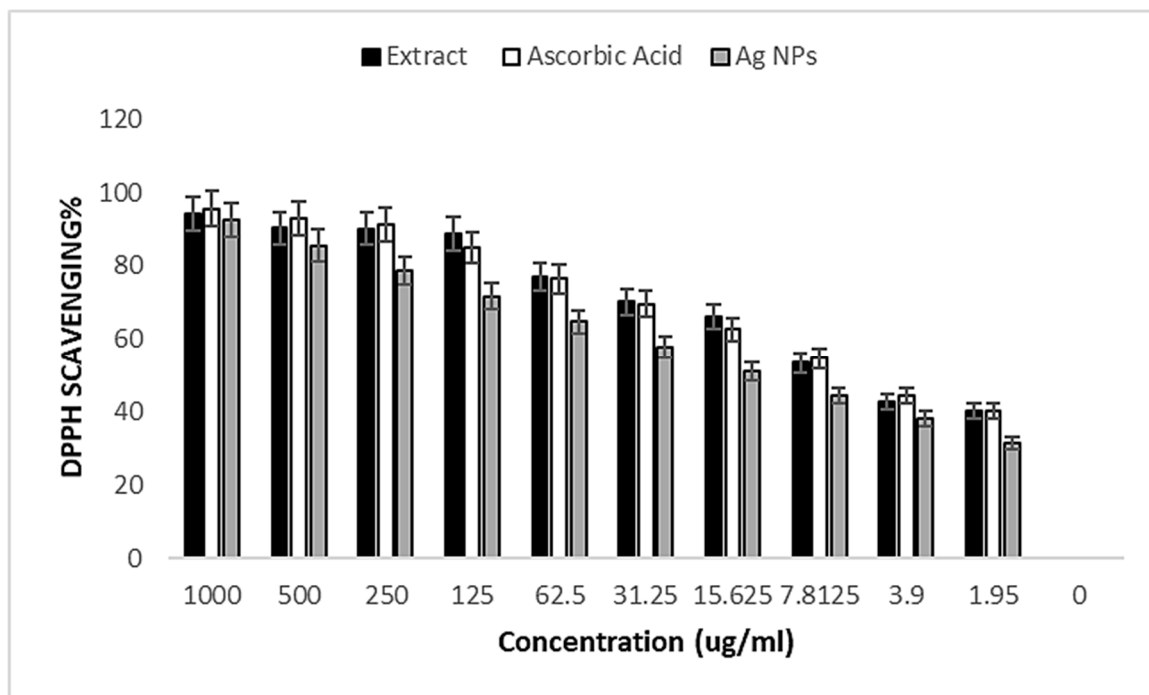


Figure 8. DPPH free-radical scavenging activity of plant extract, AgNPs, and ascorbic acid as references at different concentrations.

Using H_2O_2 models, the antioxidant capacity of AgNPs, standards, and the aqueous extract of *S. cumin* leaves was investigated. Using ascorbic acid as a reference, the H_2O_2 elimination activity of the studied materials is displayed in Table 5. AgNPs eliminated H_2O_2 at significant proportions of 93.2, 86.1, 77.8, 74.1, 66.3, 62.3, 53.2, 45, 40.3, and 37.1%, equivalent to an average IC_{50} value of 13.54 $\mu g/mL$ at varied concentrations (1000, 500, 250, 125, 62.5, 31.25, 15.625, 7.8125, 3.9, and 1.95 $\mu g/mL$). These activities, however, paled in comparison to ascorbic acid's (IC_{50} 3.45 $\mu g/mL$). With an IC_{50} value of 27.20 $\mu g/mL$, the pure plant extract had a greater inhibitory effect than Ag NP and a lower one than ascorbic acid at the same concentrations (Figure 9 and Table 5).

Table 4. DPPH free-radical scavenging activity of plant extract, AgNPs, and ascorbic acid as references at different concentrations.

Concentration	Crude Extract	Ascorbic Acid	AgNPs
1000	94.1	95.5	92.5
500	90.2	92.9	85.5
250	90.1	91.1	78.7
125	88.7	84.9	71.7
62.5	77.1	76.4	64.7
31.25	70.2	69.6	57.8
15.625	66.1	62.6	51.1
7.8125	53.5	54.7	44.4
3.9	42.8	44.3	38.1
1.95	40.3	40.2	31.4
0	0	0	0

Table 5. H₂O₂ free-radical scavenging activity of plant extract, AgNPs, and ascorbic acid as references at different concentrations.

Concentration	Crude Extract	Ascorbic Acid	AgNPs
1000	94.1	93.7	93.2
500	90.5	90.4	86.1
250	78.6	80.6	77.8
125	76.7	88.4	74.1
62.5	70.6	72.5	66.3
31.25	65.1	65.1	62.3
15.625	65.4	66.4	53.2
7.8125	48.8	55.2	45
3.9	45.6	46.2	40.3
1.95	41.1	42.3	37.1
0	0	0	0

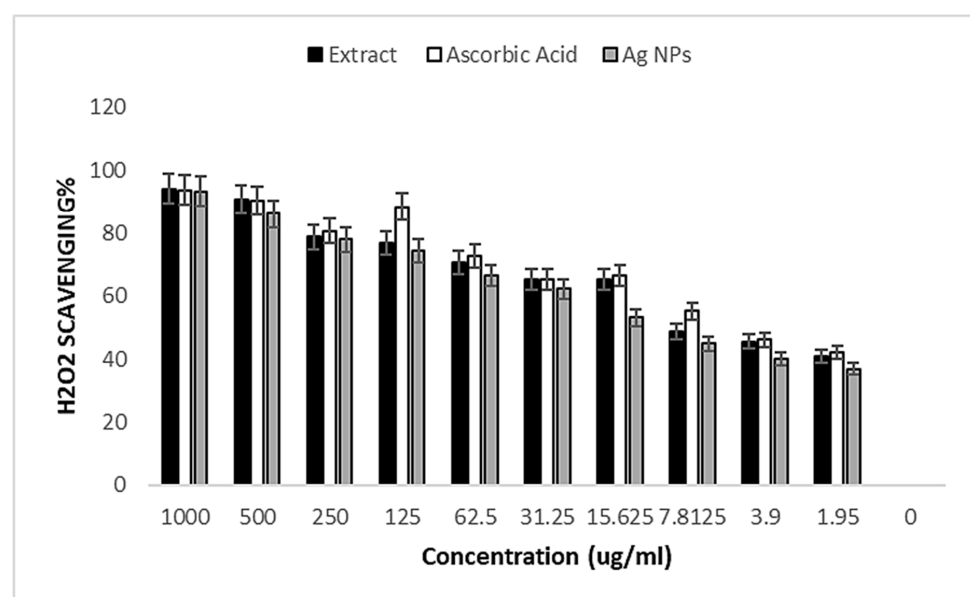


Figure 9. H₂O₂ free-radical scavenging activity of plant extract, AgNPs, and ascorbic acid as references at different concentrations.

3.6. Anti-Inflammatory Activity

The *in vitro* anti-inflammatory activity was studied using protein denaturation and the (human red blood cell) HRBC membrane hemolysis method. The green synthesized AgNPs were also evaluated for their anticoagulant activity without significant hemolytic activity on RBCs. Different concentrations of AgNPs were tested (1000, 800, 600, 400, 200, and 100 $\mu\text{g}/\text{mL}$), and they recorded 4.8, 10.2, 12.8, 14.9, 19.5, and 22.4 hemolytic inhibition%, respectively. These values were lower than all values recorded with reference to Table 6 and Figure 10.

Table 6. Anti-inflammatory effects of different AgNP concentrations against reference accompanied by low hemolytic activity.

Concentration	Anti-Inflammatory—AgNPs	Anti-Inflammatory—Indo	Hemolysis Inhibition%—AgNPs	Hemolysis Inhibition%—Indo
0	1.972	1.972	0	0
1000	0.135	0.027	95.2	99.6
800	0.225	0.056	89.8	97.8
600	0.272	0.076	87.2	96.5
400	0.307	0.092	85.1	95.5
200	0.393	0.103	80.5	94.8
100	0.446	0.115	77.6	94.2

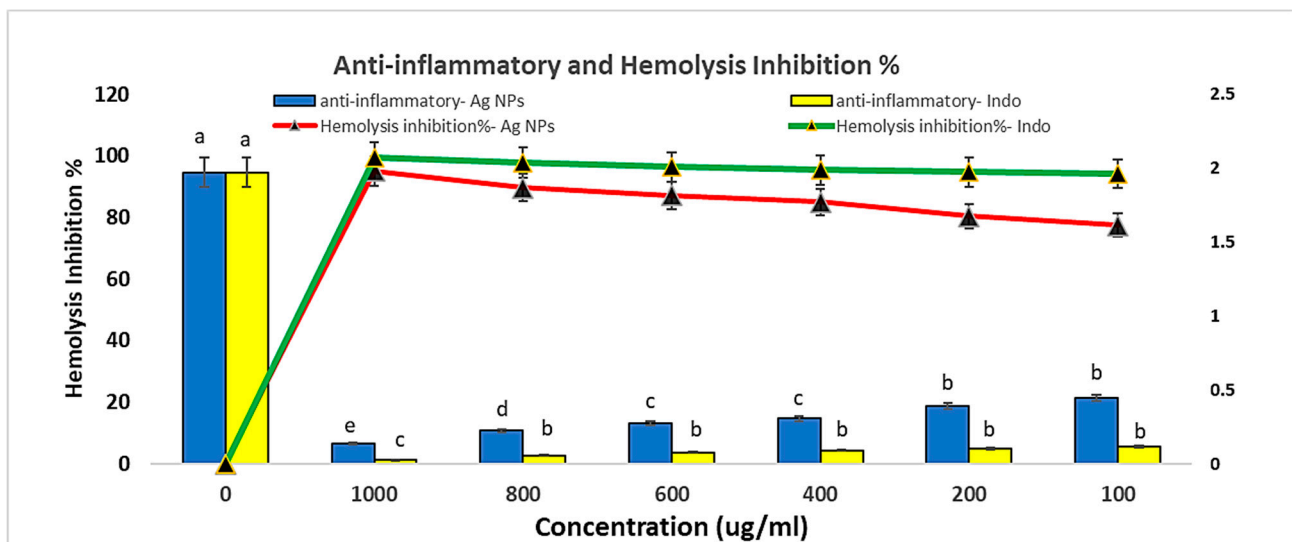


Figure 10. Anti-inflammatory effects of different AgNPs concentrations against reference accompanied by low hemolytic activity. Means with dissimilar superscript letters are significantly different at $p < 0.05$.

3.7. Antimicrobial Activity of AgNPs

AgNPs were effective antibacterial agents against MDR Gram-positive strains such as *Staphylococcus aureus*, Gram-negative strains like *Klebsiella pneumoniae*, and *Acinetobacter baumannii*, along with their antifungal effects against *Candida auris* and *Aspergillus niger* (Figure 11). The maximum inhibition activity of AgNPs was demonstrated against *Staphylococcus aureus* with 31 ± 0.81 mm at MIC 4 mg/mL and MBC 8 mg/mL, followed by *Aspergillus niger* with 30 ± 0.53 mm at MIC 16 mg/mL and MFC 32 mg/mL, then *Klebsiella pneumoniae*, *Enterococcus faecalis*, and *Acinetobacter baumannii* with 29 ± 0.61 mm, at MIC 8 mg/mL and MBC 16 mg/mL, while the minimal inhibition was against *Candida auris*

with 25 ± 0.45 mm at MIC 16 mg/mL and MFC 32 mg/mL (Figures 12 and 13). Ag nitrate has antimicrobial activity, but is lower than AgNPs, with all tested strains except against *Candida auris*. It does not exhibit any inhibitory effect on it. When comparing the inhibitory effects of AgNPs and Ag nitrate through relative percentage, the results showed that AgNPs were more effective than Ag nitrate (20.8%) with *Acinetobacter baumannii* and *Klebsiella pneumoniae*. In the case of *Staphylococcus aureus* was 40.9%; in the case of *Enterococcus faecalis*, it was 7.4%. It reaches 50% with *Aspergillus niger*, and it reaches maximum value (100%) with *Candida auris*. Furthermore, AgO NPs at a concentration of 1 $\mu\text{g/mL}$ reduced the growth of several pathogenic bacterial strains, including *Streptococcus* sp., *Bacillus* sp., *Staphylococcus* sp., *E. coli*, *Klebsiella* sp., *Shigella* sp., and *Pseudomonas aeruginosa*, in addition to one fungus, *Candida* sp. The aqueous extract of *Solanum lycopersicum* did not display any significant antimicrobial activity at the tested concentrations.

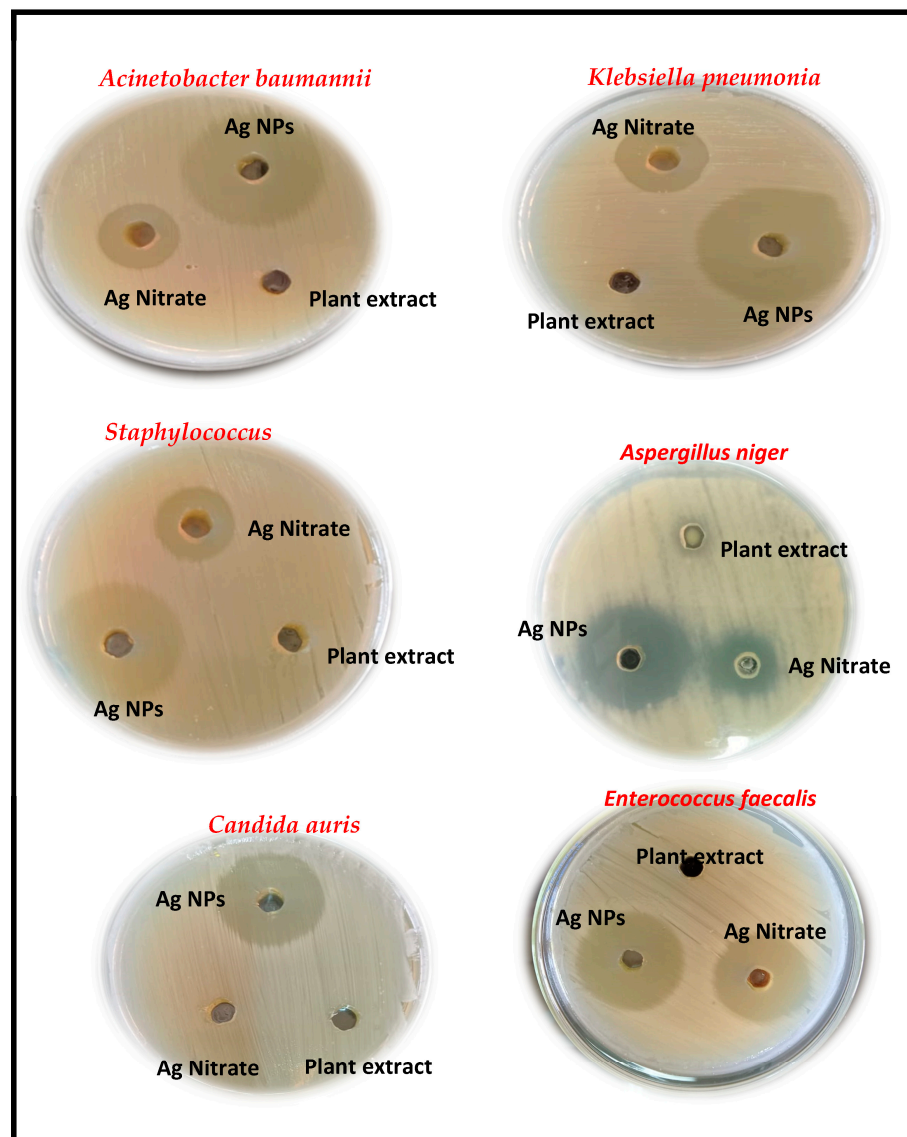


Figure 11. Inhibition zone diameter (mm) in the growth of *Staphylococcus aureus*, *Klebsiella pneumoniae*, *Acinetobacter baumannii*, *Enterococcus faecalis*, *Candida auris*, and *Aspergillus niger* through the agar well-diffusion method for 24 h of incubation against AgNPs, plant extract (*Solanum lycopersicum*), and silver nitrate.

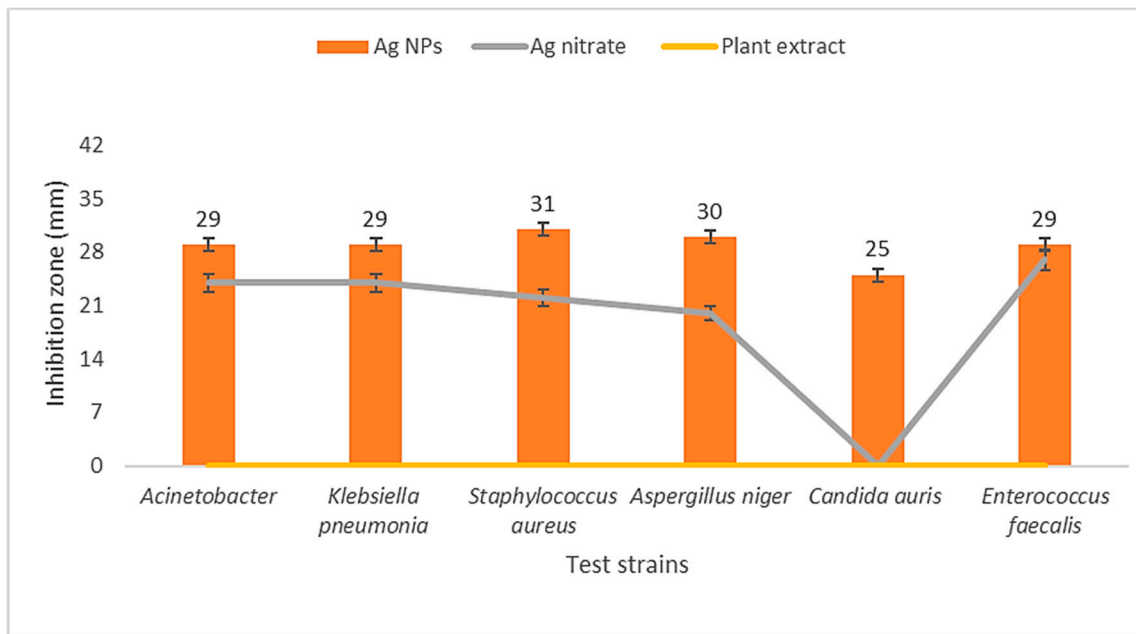


Figure 12. Inhibition zone diameter (mm) of AgNPs, Ag nitrate, and plant extract against five tested MDR bacterial and fungal strains.

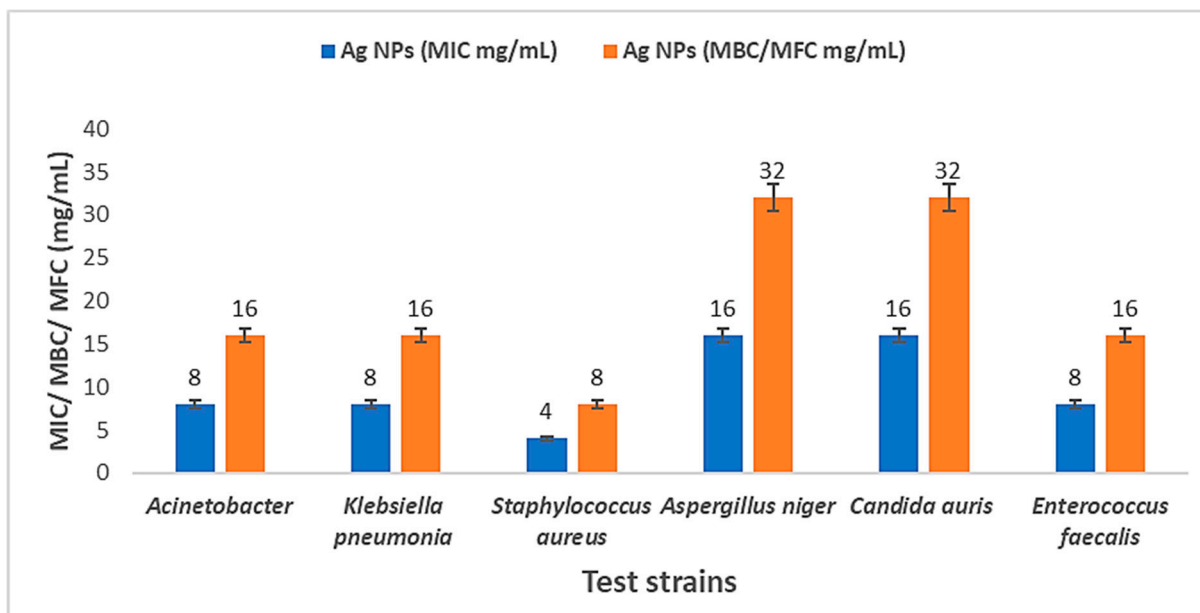


Figure 13. MIC, MBC, and MFC of AgNPs against five tested strains.

3.8. Phytochemical Analysis

A complete chemical analysis of plant extract was completed after extract preparation, as described by Alsamman et al. [33]. The detection tests for each component, such as carbohydrates, fixed oils, fats, phenol, and tannins, were conducted. It also contains flavonoids and glycosides, in addition to sterols, as summarized in Table 7. Our chemical analysis showed the presence of different active organic components in the plant extract, which concluded in Figure 14 that rutin was 88.3 mg/g, garlic acid was 70.4 mg/g, and tannic acid was 23.7 mg/g.

Table 7. The preliminary phytochemical screening of *S. cumin*.

<i>S. cumin</i> Extracted by Alcohol		
Constituents	Tests	Results
Carbohydrates	Molisch’s test	+
Fixed Oils and Fats	Saponification test	+
Phenol	Ferric chloride test	+
Tannins	Ferric chloride test	+
Phlobatannins	HCL test	–
Flavonoids	Lead acetate test	+
	AlCl ₃ test	+
Saponins	Froth test	–
Glycosides	Glycosides test	+
	Conc. H ₂ SO ₄ test	+
Alkaloids	Dragendroff’s test	–
	Wagner’s test	–
	Hager’s test	–
Sterols	Salkawskis test	+
Cardiac glycosides	Legal’s test	–
	Keller Killini test	–

(+ve) mean present, (–ve) mean absent.

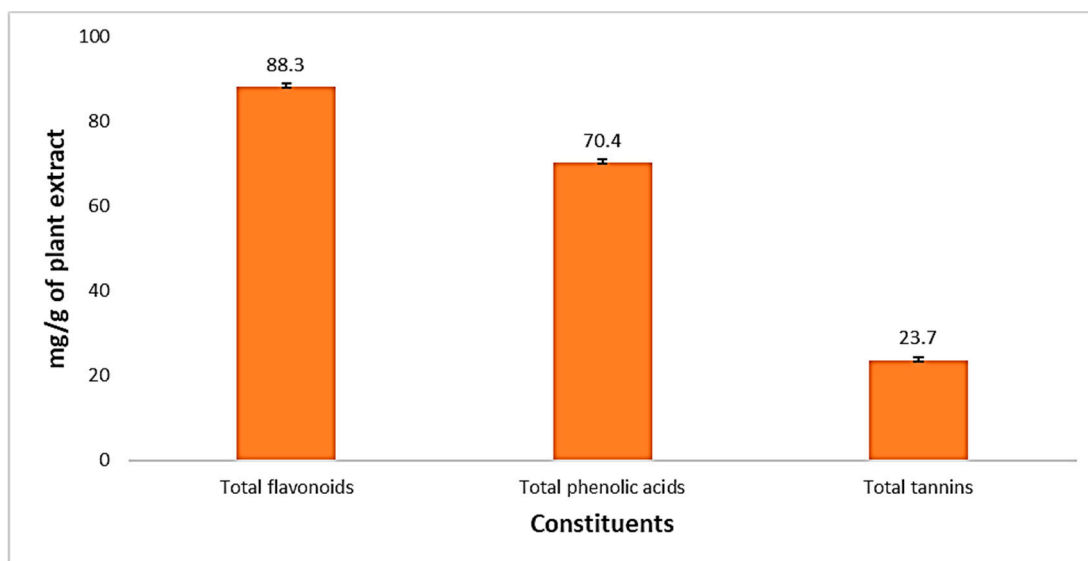


Figure 14. Percentages of total active constituents of *S. cumin* extract through the alcoholic extraction method.

3.9. Antibiofilm, Cna, and FnbA Virulence Gene Expression

AgNPs showed high values of anti-biofilm formation activity in comparison with positive control samples against four MDR bacterial isolates. Anti-biofilm was mostly effective against *Acinetobacter baumannii* with 1.99, followed by *Staphylococcus aureus* with 2.15, *Enterococcus faecalis* with 2.51, and finally *Klebsiella pneumonia* with 2.6 (Figure 15).

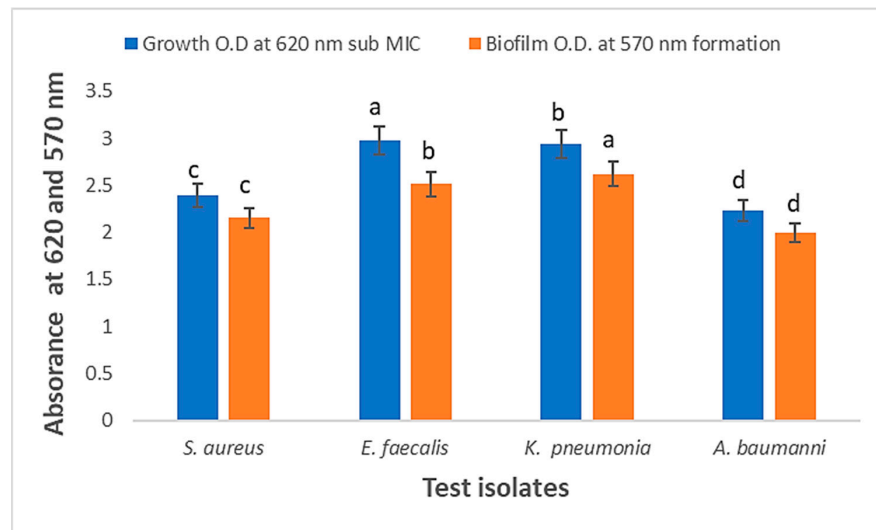


Figure 15. Anti-biofilm formation activity of AgNPs against four MDR isolates through absorbance at 570 nm. Means with dissimilar superscript letters are significantly different at $p < 0.05$.

AgNPs had little impact on the biofilm that Gram-negative bacteria formed; their values ranged from 22 to 40.17 mm. Nonetheless, our biosynthesized silver nanoparticles were not as effective against the tested Gram-positive bacteria’s biofilm; 64.85 and 59.13% of the inhibitory effect on biofilm were found against *Candida albicans* and *Candida sake*, respectively; the maximum inhibitory effect was found against *Candida* species [71]. The high biofilm-suppression activity of silver nanoparticles was demonstrated against *S. aureus*, *Bacillus subtilis*, and *Pseudomonas aeruginosa* [72]. In our research, plant-synthesized AgNPs also cause the downregulation of two fundamental genes for biofilm formation in *S. aureus*. First, total RNA was extracted and then purified, followed by reverse transcription for mRNA. Then, cDNA was used as a template for dsDNA sequences of genes of interest, and a final step aimed at partial sequencing of our genes. A *RecA* partial sequence showed about 1400 bps, *cna* was estimated with 1200 pbs, while *fnbA* was partially estimated at 1K bps (Figure 16). Gene expression exhibits that *fnbA* was depressed in its expression by 6-fold, while another one, *Cna*, was depressed in its expression by 12.5-fold when compared with the housekeeping gene *RecA*. This was analyzed through dd Δ ct, in which *RecA* gene expression was used as the standard, as it is one of the housekeeping genes against which were tested two genes of biofilm, *Cna* and *fnbA* (Figure 17).

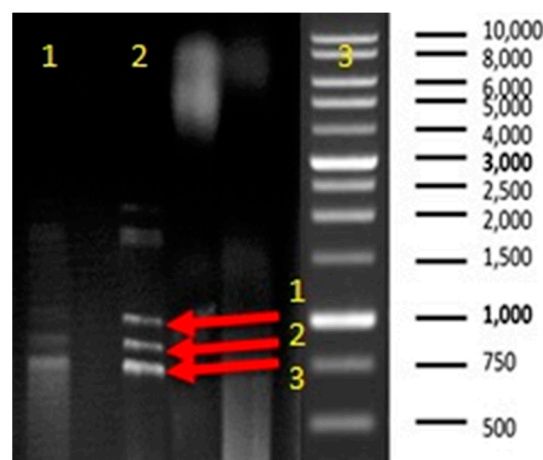


Figure 16. RT-PCR of the three genes within *S. aureus* line [1]: treated sample, line [2]: control sample, wherein both lines of the first band 1 represent *RecA* gene amplicon, the second band 2 represents *Cna* gene amplicon, and, finally, the third band 3 represents *FnbA* gene amplicon.

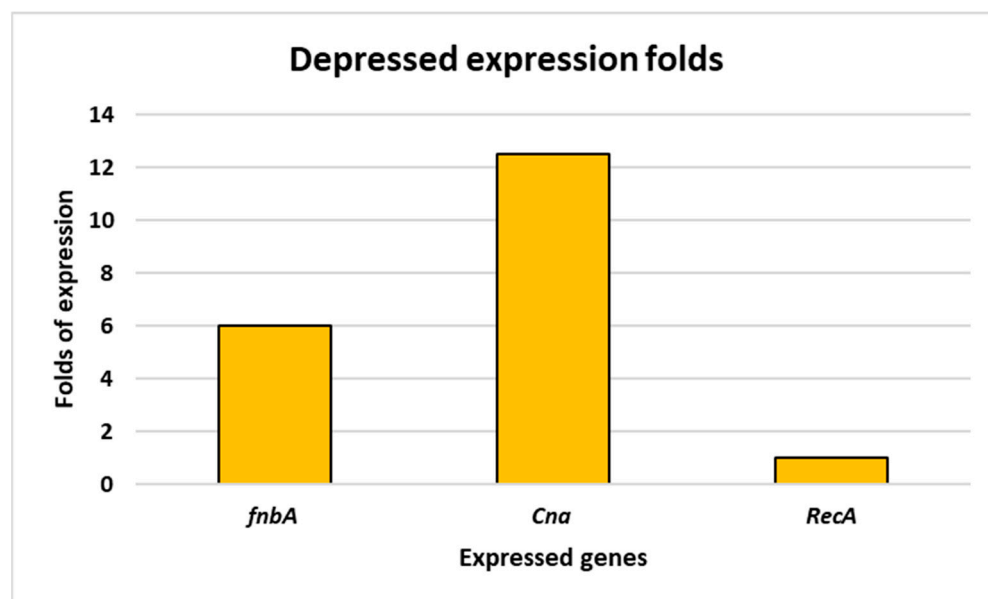


Figure 17. Gene expression in folds for RecA gene against biofilm formation genes *fnbA* and *Cna*.

4. Discussion

Plants are thought of as nature's chemical factories since they are low-maintenance and affordable. Because they generate huge amounts of phytochemicals, a variety of plant components, including fruit, leaves, stems, and roots, have been extensively employed for the environmentally friendly creation of nanoparticles [73]. Environmentally friendly technologies have been used to generate nanoparticles of silver, zinc oxide, and other materials [74–76]. Plant extracts contain phytochemicals such as polyols, terpenoids, and polyphenols, which are responsible for metallic ion bioreduction [73]. To lessen the difficulties associated with chemical and physical methods, green techniques (plants, fungi, bacteria, actinomycetes, and yeasts) are preferred for the manufacturing of metal and metal oxide NPs [16,77]. Silver ions were reduced, capped, and stabilized using tomato-leaf extracts. According to Al-Askar et al. [78], combining the zinc acetate solution with the *P. indica* aqueous extract led to the creation of white ZnONPs. Moreover, orange- and pomegranate-peel extracts have greater total phenolic contents, according to Mostafa et al. [79], which supports the reduction of silver ions to AgNPs. Ali et al. [80] biosynthesized nanosilver particles from tomato-peel extract (TPE-AgNPs) and evaluated their characteristics and inhibitory activities against pathogenic bacteria and fungi. According to Singh et al. [81], a leaf extract from *Carissa carandas* L. was used as a reducing and capping agent to accomplish the green biosynthesis of silver nanoparticles (AgNPs). On the other hand, *Rhizopus oryzae* biomass extract was used to biosynthesize silver nanoparticles [64]. Additionally, Iqbal et al. [21] prepared SeNPs by using two types of extracts of freshly prepared tomato (*Solanum lycopersicum*) fruit extract and seed extract for antibacterial and antioxidant activity. Bharathi et al. [82] synthesized FeONPs from *Solanum lycopersicum*-leaf extract and showed potential antibacterial activity against *Escherichia coli*. They also showed significant in vitro anticancer activity against the human lung cancer cell line A549. Elbrolesy et al. [83], investigated the biosynthesis of ZnO NPs using *Solanum lycopersicum*-leaf extract for evaluation of their antibacterial and anticancer activity. Rodríguez-Varillas et al. [84] obtained carbon dots from tomato juice (*Solanum lycopersicum*) in order to obtain nanoparticles with antioxidant capabilities.

The AgNPs' absorption characteristics are mostly determined by the size and shape of the particles. The typical size of NPs is reflected in the SPR range for AgNPs, which is 380–450 [85]. Nallal et al. [86] proposed the efficient and quick synthesis of AgNPs by sunlight using an extract of *A. ampeloprasum*; the creation of AgNPs was verified by an absorption peak in the UV–Vis spectrum at 446 nm. Singh et al. [81] biosynthesized AgNPs

at 432 nm and 444 nm for reactions carried out at 25 °C and 60 °C, respectively. Conversely, higher concentrations of AgNPs and lower average AgNP sizes are linked to higher and lower maximum wavelength values, respectively [87]. El-Bendary et al. [88] detected a peak in the AgNPs spectra at 410 nm, providing evidence that AgNPs were produced by *Aspergillus caespitosus*. Here, Hashem et al. [42] produced AgNPs by *B. thuringiensis* MAE 6 and had an SPR absorption band at 420 nm. Pallavi et al. [89] reported that the generated AgNPs exhibited a clear and distinct absorption peak at 418 nm, whose broad peak absorption of UV data indicates that the culture supernatant of the *Streptomyces hirsutus* strain SNPGA-8 has reduced silver nitrate to silver nanoparticles.

Furthermore, the XRD analysis is in agreement with Saied et al. [68], who found that AgNPs are biosynthesized using *Cytobacillus firmus* and have diffraction signals (111, 200, 220, and 311). These results agree with those published in [90–92], where it was discovered that the average particle size ranged between 5 and 20 nanometers. The average particle size of the AgNPs generated by the *Streptomyces hirsutus* strain SNPGA-8 was 12.74 nm, according to Pallavi et al. [89]. El-Gamal et al. [93] demonstrated that the AgNP formation is shown by strong peaks corresponding to (111), (200), (220), and (311), which were produced by *Streptomyces* sp. MI-3, and were face-centered cubic in structure and crystallized. According to Ajitha et al. [94], AgNPs synthesized using *Syzygium aromaticum* (clove) extract had the same patterns as AgNPs created under optimal conditions. Four notable diffraction peaks were produced by the AgNPs at 2θ , 38.0°, 44.1°, 64.4°, and 77.4°. These peaks were linked to the lattice planes of the metallic silver's face-centered cubic (fcc) structure and its crystalline nature.

Additionally, the TEM image is used to detect of shape and size of biosynthesized NPs. The diameters of the nanoparticles of this study were varied from 35 to 80 nm, with an average size of 53 nm. The synthesized BT-AgNPs size varied from 20.15 to 22.21 nm, as demonstrated by Chi et al. [95]. Furthermore, the average size of the AgNPs produced by the extract of walnut fruit (*Juglans regia*) was 31.4 nm [96]. Nagaraja et al. [97] showed that the TEM picture of LnFb-AgNPs was between 10 and 45 nm in size; the TEM micrographs showed that the average particle size was 24.50 nm. Hamouda et al. [98] created spherical AgNPs with diameters ranging from 100 to 200 nm using *Oscillatoria Willei* NTDM01 extract. On the other hand, the size of spherical AgNPs synthesized by *Bacillus* sp. KFU36 was extended between 5–15 nm [99]. Another study by Lakhan et al. [99] demonstrated, that NPs synthesized using a clove-bud extract had a polydispersed nature and nanoparticle sizes ranging from 10 to 50 nm without agglomeration.

The FTIR analysis was used to detect the functional groups used as a reducing agent for NPs biosynthesis. The broad peak at 3348 cm^{-1} originated from OH groups in the saponin structure. It is also noted that these bonds may be due to the stretching of OH in proteins, enzymes, or polysaccharides present in the extract [100]. The peaks at 2966 and 2115 cm^{-1} are due to the C–H stretching of the methylene group or aliphatic group, and it is also a characteristic peak of triterpenoid saponins. The band at 1586 cm^{-1} denoted the bending vibrations of the amide I group and suggested the possibility of binding AgNPs with proteins found in the extracts [81]. Two bands observed at 1374 and 1045 cm^{-1} showed the presence of C–O stretching of phenol or tertiary alcohols; the band at 1043.27 cm^{-1} showed the O–H stretching of the phenol group [101]. Two bands at 822 and 644 cm^{-1} were because of the C–O stretch and C–S stretch, or the involvement of aliphatic chloro compounds; the band at 644 cm^{-1} might be due to the C–H stretching of the aromatic group; and the peak at 531 cm^{-1} showed the OH group of phenols [102]. Additional information has revealed that proteins may function as stability or capping agents during Ag-NP production [34,103]. According to Singh et al. [81], biomolecules involved in the reduction of Ag^+ ions and the capping of biosynthesized AgNPs were identified by analyzing the Fourier transform infrared spectra of leaf extract from *Carissa carandas* L., which mediated the production of different silver nanoparticles. An FTIR spectrum study indicates that Meena et al. [100] discovered that the aqueous leaf extract from *Cucumis prophetarum* may act as stabilizing and reducing agents while Ag-NPs are synthesized.

For molecular identification the 16S rDNA technique was used to identify of MDR Isolates. Similarly, Abdelrazik et al. [104] used 16S rDNA PCR sequencing to identify the top five MDR bacterial isolates: *Escherichia coli*, *Pseudomonas aeruginosa*, *Acinetobacter baumannii*, *Enterococcus faecalis*, and *Klebsiella pneumoniae*, with accession numbers OP741103, OP741104, OP741105, OP741106, and OP741107, respectively. Other research conducted by Khedr et al. [105] included the identification of three LAB isolates as *Lactobacillus delbrueckii* using 16S rDNA.

For the antioxidant assay, the interaction of biomolecules with molecular oxygen in biological systems produces free radicals [106]. Consequently, the ROS action is resisted by using antioxidant compounds. The AgNPs effectively showed DPPH inhibition activity, and it was found to be dose-dependent [107]. According to Shehabeldine et al. [108], who reported at doses of 4000, 2000, and 1000 $\mu\text{g}/\text{mL}$, Chi/Ag-NPs had a potential antioxidant activity of 92, 90, and 75%; their IC₅₀ was 261 $\mu\text{g}/\text{mL}$. Several bio-reductive groups of phytochemicals found on the surfaces of Ag-NPs are thought to be responsible for the highest level of antioxidant activity [108]. According to Rajivgandhi et al. [109], the antioxidant values of 0.765, 0.478, and 0.890 were observed at 250 $\mu\text{g}/\text{mL}$. The toxicity effect of AgNPs is determined and influenced by multiple factors; for example, the size-dependent toxicity effect of AgNPs was proven in a study where 10 nm particles portrayed significantly greater toxicity compared to 50 nm, 100 nm, and 200 nm particles. Meanwhile, the shape-dependent toxicity of AgNPs was illustrated in a comparative study on the effect of silver wires (diameter 100–160 nm), spherical silver nanoparticles (30 nm), and silver microparticles (<45 μm) synthesized by wet chemical methods on human alveolar epithelial cells (A549). Based on the results reported, reduction of cell viability and increased lactic acid dehydrogenase (LDH) release by silver wires were observed, while spherical AgNPs showed no such effects. So, we concluded that AgNPs are suitable to be included in a wound-healing formulation up to 25 $\mu\text{g}/\text{mL}$. The total antioxidant activity [110] of the synthetic AgNPs was observed by Dridi et al. [111] to be similar to that of the standard, gallic acid. AgNPs demonstrated a greater capacity to scavenge DPPH than ascorbic acid, indicating their antiradical action (13.08 IP) with an inhibition percentage of 5.09. When compared to ascorbic acid, which had a ferric antioxidant reduction power of 0.66, these manufactured AgNPs show a higher one of 9.46 mg EAA/g DM. Similar findings were reported by Rajeshkumar et al. [112], who discovered that the antioxidant and DPPH free-radical scavenging activities were increased more by the seaweed synthesis of NPs than by crude extract. Pfp-AgNPs biosynthesized by Govindappa et al. [113] had shown better H₂O₂ and DPPH scavenging activities, which might have been due to the structure, characterization, and type of capping agents. In another study, the biogenic AgNPs inhibited $69.73 \pm 0.56\%$ of DPPH free radicals at 500 $\mu\text{g mL}^{-1}$, indicating considerable antioxidant potential [114].

Another feature of green synthesized AgNPs, aside from the most common ones, is their anti-inflammatory effect [115]. Inflammation is a complicated process that is mostly accompanied by elevated blood vessel permeability, increased protein denaturation, and changes in the cellular membrane. When protein denaturation occurs, they lose their secondary and tertiary structures as a result of heat or stress, resulting in inflammation [116]. Any chemical could be divided into three distinct groups based on its hemolytic impact, according to the American Society for Testing and Materials [117]: hemolytic (hemolysis greater than 5%), mild hemolysis (between 2% and 5%), and no hemolysis (less than 2%) [118]. Using the chemical quercetin, Chahardoli et al. [119] investigated the anti-inflammatory effect of biosynthesized AgNPs and found comparable outcomes. The biosynthesized NPs exhibited 100% anti-inflammatory efficacy, which can be attributed to the coating agent quercetin present on their surface. In another study, protein denaturation is a perfectly documented reason for the inflammation in conditions such as rheumatoid arthritis. The prevention of protein denaturation is the main mechanism of action of nonsteroidal anti-inflammatory drugs (NSAIDs) [120]. The biogenic silver nanoparticles biosynthesized by Sabarathinam et al. [121] show comparable anti-inflammatory activity

with standard diclofenac sodium, which is a chemical analgesic at a 50 microL concentration and can act as a potent anti-inflammatory drug. It is commonly known that the mechanism of action of protein denaturation inhibitors is the suppression of several inflammatory mediators involved in the inflammatory process [122]. Drugs including phenylbutazone, salicylic acid, sodium diclofenac, and flufenamic acid exhibit dose-dependent efficacy against protein denaturation, which is a well-documented source of inflammation [123]. Additionally, it has been noted that a variety of plant extracts and the separated chemicals from them had strong anti-inflammatory action that was on par with that of synthetic anti-inflammatory medications. The majority of anti-inflammatory drugs stabilize the plasma membrane of mammalian erythrocytes and thereby inhibit heat-induced and hypotonicity-induced hemolysis [123,124]. Additionally, In vitro, AgNPs are thought to have anti-inflammatory effects, as they play a role in the wound-curing process by TNF- α , interferon, and interleukin-1, as well as by inhibiting COX-2 besides MMP-3 expression. They may diminish the activity of TNF- α , which is involved in inflammatory processes [125,126]. Chi et al. [127] discovered that the kernel-fabricated silver nanoparticles possess a reasonable anti-inflammatory (69.77%).

For antimicrobial activity, The *Enterobacteriales* order, which includes Gram-negative bacteria found in the intestine, like *Escherichia coli* and *Klebsiella* spp., is known to cause UTIs. Other pathogens include nonfermenting Gram-negative bacteria like *Pseudomonas* spp. and *Acinetobacter* spp., atypical microorganisms like *Mycoplasma* and *Ureaplasma* species, and yeast (*Candida* spp.) [128–130].

Similarly, Loo et al. [131] observed that AgO NPs minimum inhibitory concentration (MIC) against *Salmonella typhimurium*, *Escherichia coli*, *Klebsiella pneumoniae*, and *Salmonella enteritidis* was 7.8, 3.9, 3.9, and 3.9 $\mu\text{g}/\text{mL}$, in that order. AgO NPs' bactericidal activity has been evaluated using growth curves at doses ranging from 0 to 8 \times MIC dilution factor [33]. Khaydarov et al. [132] and Yousef et al. [133] reported that the AgNPs MIC values for *S. aureus* and *Enterococcus faecalis* were 3 and 2 mg/mL , respectively. Alsamman et al. [33] reported that AgO NPs exhibit maximum antibacterial activity among the selected five MDR-tested isolates, with TiO₂ nanoparticles being the second most effective type. Microbial AgO had an average size of 30 nm by TEM with a smooth and regular spherical shape, while plant-mediated AgO NPs had an average size of 52 nm as demonstrated by TEM examination. AgO and TiO₂ showed notable antibacterial activity for all the MDR isolates tested, especially against *E. coli* and *Staphylococcus sciuri* [33]. The findings, determined by Sharifi-Rad et al. [120], demonstrate the antibacterial activity of the *A. tribuloides* root extract and the greenly synthesized AgNPs against the Gram-positive (*B. cereus* and *S. aureus*) and Gram-negative bacterial strains (*E. coli* and *Sh. flexneri*) at comparable concentrations (500 $\mu\text{g}/\text{mL}$). It was discovered that strains of bacteria were significantly inhibited by the *A. tribuloides* root extract and the environmentally produced AgNPs. In contrast to Gram-positive bacteria strains, AgNPs showed more inhibition action against Gram-negative bacteria, whereas *A. tribuloides* root extract demonstrated greater inhibition activity against Gram-positive bacteria. The TPE-AgNPs from tomato peels (*Solanum lycopersicum*) obtained by Ali et al. [80] showed that *B. subtilis* and *E. coli* were the most sensitive pathogens, with IZDs of 4.0 and 0.92 cm, respectively. However, *L. monocytogenes* and *S. sonnei* were the most resistant pathogens, with IZDs of 0.92 and 0.90 cm, respectively. The synthesized TPE-AgNPs from tomato peels had good inhibitory potentials against pathogenic fungi, with IZDs of 3.0 and 0.92 cm against *A. solani* and *C. albicans*, respectively.

The high antibacterial activity of AgNPs is attributable to their large surface area, which provides better contact of the nanoparticles with the cell walls of microorganisms [134]. The biosynthesized AgNPs functioned through the mechanisms of increased affinity for sulfur proteins and electrostatic attraction caused by silver ions that could cling to the cytoplasmic membrane and cell wall. The bacterial envelope may be disturbed due to the associated ions' potential to enhance the cytoplasmic membrane's permeability [135]. As lipid peroxidation increases, cellular reducing sugars and total proteins flow through

damaged cell membranes [136]. DNA replication and cell reproduction can be affected by the interaction between silver ions and the sulfur and phosphorus in DNA. Silver ions also have the ability to stop the synthesis of proteins by denaturing ribosomes in the cytoplasm [137]. Additionally, the dissolution of AgNPs releases antimicrobial silver ions, which actively interact with thiol-containing proteins within the cellular wall and affect their functionality. Upon interaction with the outer membrane, AgNPs are capable of binding with proteins and forming complexes with electron donors containing oxygen, phosphorus, nitrogen, or sulfur atoms [138,139].

For the phytochemical analysis, a complete chemical analysis of plant extract was examined. The findings reported by Mohammed et al. [140] show that the qualitative phytochemical analysis showed that while carbohydrates, steroids, and anthroquinone were absent from both the healthy and infected leaves of *Solanum lycopersicum*, alkaloids, flavonoids, tannins, cardiac glycosides, phenols, and saponins were present. The quantitative study showed that both healthy and infected leaf curls of *Solanum lycopersicum* contained 8.2% and 3.8% alkaloids, 49.6% and 48.2% flavonoids, 30.6% and 19.99% tannins, 13.6% and 7.022% phenols, and 1.2% and 0.1% saponins. According to Mehmood et al. [141], who evaluated the phytochemicals of black-cumin extracts, they confirmed the occurrence of flavonoids, alkaloids, phenols, and tannins. Also, the bioactive components of the ethanolic extracts of five popular Indian seed spices—coriander, cumin, fenugreek, fennel, and black cumin—were qualitatively analyzed. These extracts' qualitative phytochemical assays reveal the presence of many phytochemicals, including anthocyanin, steroid, flavonoid, saponin, tannin, alkaloid, and coumarin. The most prevalent phytochemical found in all of the seed spices was an alkaloid. Notably absent are coumarins and steroids, with the exception of black cumin and fenugreek, respectively [142]. According to Balaram et al. [143], who determined the phytochemicals of *Cuminum cyminum*, screening shows the presence of phytochemicals like alkaloids, glycosides, steroids, flavonoids, tannins, saponins, resins, and phenols.

5. Conclusions

In conclusion, our study presents a simple and cost-effective method for synthesizing biogenic Ag nanoparticles (NPs) using *Solanum lycopersicum* (*S. cumin*), commonly known as tomato. Through UV–visible spectroscopy, XRD, and TEM analyses, we characterized the biosynthesized AgNPs, observing a maximum surface plasmon resonance (SPR) at 457 nm. TEM imaging revealed particle diameters ranging from 5 to 30 nm, while XRD analysis confirmed their crystalline nature, with an average size of 55 nm. Importantly, these AgNPs exhibited significant antimicrobial activity against a variety of pathogens, including unicellular and multicellular fungi and Gram-positive and Gram-negative bacteria. AgNPs showed inhibition activity against *S. aureus*, with 31 mm at MIC 4 mg/mL and MBC 8 mg/mL, followed by *A. niger* with 30 mm at MIC 16 mg/mL and MFC 32 mg/mL, then *E. faecalis*, *K. pneumonia* and *A. baumannii* with 29 mm, at MIC 8 mg/mL and MBC 16 mg/mL, while the minimal inhibition was against *C. auris* with 25 mm at MIC 16 mg/mL and MFC 32 mg/mL. Additionally, the AgNPs demonstrated antioxidant properties, effectively scavenging DPPH and H₂O₂ radicals (AgNPs at different concentrations removed DPPH and H₂O₂ at IC₅₀ value of 13.54 µg/mL) and influencing the downregulation of critical genes involved in biofilm formation in *S. aureus*, indicating potent antibiofilm activity. AgNPs concentrations in the range of 3–6 mg/mL showed decreased expression of two of the fundamental genes necessary for biofilm formation within *S. aureus*, *fnbA* (6-fold) and *Cna* (12.5-fold) when compared with the *RecA* gene, which decreased by one-fold when compared with the control sample. The results showed that both tomato-leaf extract and biosynthesized AgNPs have remarkable antimicrobial, antibiofilm, antioxidant, and anti-inflammatory activity, although the AgNPs effect was greater than that of tomato-leaf extract in these activities. In addition, two genes of biofilm formation in *S. aureus*, *Cna*, and *FnbA* were depressed with AgNPs.

For future research, several avenues are suggested.

1. Further investigation into the mechanisms through which AgNPs exert their antimicrobial and antibiofilm effects could yield valuable insights, enabling the optimization of their efficacy and specificity;
2. Assessing the effectiveness and safety of biosynthesized AgNPs in animal models is essential for the translation of these findings into practical applications;
3. Investigating the synergistic effects of AgNPs with existing antibiotics or antimicrobial agents could present new strategies for combating microbial resistance;
4. Evaluating the potential of AgNPs for environmental disinfection and as coatings for medical devices could broaden their use in preventing microbial contamination and healthcare-associated infections;
5. Further research into how AgNPs affect the expression of genes involved in microbial virulence and resistance mechanisms could improve our understanding of their comprehensive antimicrobial properties.

Overall, the development of biogenic AgNPs from *Solanum lycopersicum* represents a promising path for enhancing antimicrobial strategies, necessitating ongoing research to fully exploit their potential in both clinical and environmental applications.

Author Contributions: Conceptualization, A.E.M., S.A.E. and M.K.; Methodology, A.E.M., A.E.M.A., F.S.Y., A.A.S., E.A.A., M.A.G., A.M.A., G.A. and R.A.S.; Software, A.M.A. and E.S.; Validation, S.A.E. and E.A.A.; Formal analysis, A.E.M.A., F.S.Y., A.A.A.-A., M.A.S., E.S. and M.K.; Investigation, S.A.E., A.A.S., M.A.G., A.Y., G.A. and M.A.S.; Resources, A.E.M., A.E.M.A., A.A.S., A.A.A.-A., A.Y., R.A.S. and M.A.S.; Data curation, F.S.Y. and E.A.A.; Writing—original draft, A.E.M., A.E.M.A. and M.K.; Writing—review & editing, E.S. and M.K.; Visualization, M.A.G. and M.K. All authors have read and agreed to the published version of the manuscript.

Funding: The authors extend their appreciation to the researchers supporting project number (RSP2024R505), King Saud University, Riyadh, Saudi Arabia.

Institutional Review Board Statement: The study was conducted in accordance with the Declaration of Helsinki, and approved by the Institutional Review Board (or Ethics Committee) of El-Menoufia University (IRB approval number and date 12/2023MICR4-2) (1 January 2023) for studies involving humans.

Informed Consent Statement: Informed consent was obtained from all subjects involved in the study.

Data Availability Statement: The data presented in this study are available on request from the corresponding author.

Acknowledgments: The authors extend their appreciation to the researchers supporting project number (RSP2024R505), King Saud University, Riyadh, Saudi Arabia.

Conflicts of Interest: The authors declare no conflict of interest.

References

1. Öztürk, R.; Murt, A. Epidemiology of urological infections: A global burden. *World J. Urol.* **2020**, *38*, 2669–2679. [[CrossRef](#)] [[PubMed](#)]
2. Zagaglia, C.; Ammendolia, M.G.; Maurizi, L.; Nicoletti, M.; Longhi, C. Urinary tract infections caused by uropathogenic *Escherichia coli* strains—New strategies for an old pathogen. *Microorganisms* **2022**, *10*, 1425. [[CrossRef](#)] [[PubMed](#)]
3. Xu, L.; Wang, Y.-Y.; Huang, J.; Chen, C.-Y.; Wang, Z.-X.; Xie, H. Silver nanoparticles: Synthesis, medical applications and biosafety. *Theranostics* **2020**, *10*, 8996. [[CrossRef](#)] [[PubMed](#)]
4. Bunduki, G.K.; Heinz, E.; Phiri, V.S.; Noah, P.; Feasey, N.; Musaya, J. Virulence factors and antimicrobial resistance of uropathogenic *Escherichia coli* (UPEC) isolated from urinary tract infections: A systematic review and meta-analysis. *BMC Infect. Dis.* **2021**, *21*, 753. [[CrossRef](#)]
5. Guliciuc, M.; Porav-Hodade, D.; Mihailov, R.; Rebegea, L.-F.; Voidazan, S.T.; Ghirca, V.M.; Maier, A.C.; Marinescu, M.; Firescu, D. Exploring the Dynamic Role of Bacterial Etiology in Complicated Urinary Tract Infections. *Medicina* **2023**, *59*, 1686. [[CrossRef](#)] [[PubMed](#)]
6. Terreni, M.; Taccani, M.; Pregnolato, M. New antibiotics for multidrug-resistant bacterial strains: Latest research developments and future perspectives. *Molecules* **2021**, *26*, 2671. [[CrossRef](#)]

7. Mohamed, A.H.; Sheikh Omar, N.M.; Osman, M.M.; Mohamud, H.A.; Eraslan, A.; Gur, M. Antimicrobial resistance and predisposing factors associated with catheter-associated UTI caused by uropathogens exhibiting multidrug-resistant patterns: A 3-year retrospective study at a tertiary Hospital in Mogadishu, Somalia. *Trop. Med. Infect. Dis.* **2022**, *7*, 42. [[CrossRef](#)] [[PubMed](#)]
8. Hugon, P.; Dufour, J.-C.; Colson, P.; Fournier, P.-E.; Sallah, K.; Raoult, D. A comprehensive repertoire of prokaryotic species identified in human beings. *Lancet Infect. Dis.* **2015**, *15*, 1211–1219. [[CrossRef](#)]
9. Upadhayay, A.; Ling, J.; Pal, D.; Xie, Y.; Ping, F.-F.; Kumar, A. Resistance-proof antimicrobial drug discovery to combat global antimicrobial resistance threat. *Drug Resist. Updat.* **2023**, *66*, 100890. [[CrossRef](#)]
10. Ahmed, S.F.; Mofijur, M.; Rafa, N.; Chowdhury, A.T.; Chowdhury, S.; Nahrin, M.; Islam, A.S.; Ong, H.C. Green approaches in synthesising nanomaterials for environmental nanobioremediation: Technological advancements, applications, benefits and challenges. *Environ. Res.* **2022**, *204*, 111967. [[CrossRef](#)]
11. Gour, A.; Jain, N.K. Advances in green synthesis of nanoparticles. *Artif. Cells Nanomed. Biotechnol.* **2019**, *47*, 844–851. [[CrossRef](#)] [[PubMed](#)]
12. Barhoum, A.; García-Betancourt, M.L.; Jeevanandam, J.; Hussien, E.A.; Mekkawy, S.A.; Mostafa, M.; Omran, M.M.; Abdalla, M.S.; Bechelany, M. Review on natural, incidental, bioinspired, and engineered nanomaterials: History, definitions, classifications, synthesis, properties, market, toxicities, risks, and regulations. *Nanomaterials* **2022**, *12*, 177. [[CrossRef](#)]
13. Bruna, T.; Maldonado-Bravo, F.; Jara, P.; Caro, N. Silver nanoparticles and their antibacterial applications. *Int. J. Mol. Sci.* **2021**, *22*, 7202. [[CrossRef](#)] [[PubMed](#)]
14. Stabryla, L.M.; Johnston, K.A.; Millstone, J.E.; Gilbertson, L.M. Emerging investigator series: It's not all about the ion: Support for particle-specific contributions to silver nanoparticle antimicrobial activity. *Environ. Sci. Nano* **2018**, *5*, 2047–2068. [[CrossRef](#)]
15. Mba, I.E.; Nweze, E.I. Nanoparticles as therapeutic options for treating multidrug-resistant bacteria: Research progress, challenges, and prospects. *Biotechnology* **2021**, *37*, 108. [[CrossRef](#)] [[PubMed](#)]
16. Jeevanandam, J.; Kiew, S.F.; Boakye-Ansah, S.; Lau, S.Y.; Barhoum, A.; Danquah, M.K.; Rodrigues, J. Green approaches for the synthesis of metal and metal oxide nanoparticles using microbial and plant extracts. *Nanoscale* **2022**, *14*, 2534–2571. [[CrossRef](#)] [[PubMed](#)]
17. Younessi-Hamzekhanlu, M.; Ozturk, M.; Jafarpour, P.; Mahna, N. Exploitation of next generation sequencing technologies for unraveling metabolic pathways in medicinal plants: A concise review. *Ind. Crop. Prod.* **2022**, *178*, 114669. [[CrossRef](#)]
18. Elshafie, H.S.; Camele, I.; Mohamed, A.A. A Comprehensive review on the biological, agricultural and pharmaceutical properties of secondary metabolites based-plant origin. *Int. J. Mol. Sci.* **2023**, *24*, 3266. [[CrossRef](#)]
19. Liu, L.; Yu, C.; Ahmad, S.; Ri, C.; Tang, J. Preferential role of distinct phytochemicals in biosynthesis and antibacterial activity of silver nanoparticles. *J. Environ. Manag.* **2023**, *344*, 118546. [[CrossRef](#)]
20. Parmar, S.; Kaur, H.; Singh, J.; Matharu, A.S.; Ramakrishna, S.; Bechelany, M. Recent advances in green synthesis of AgNPs for extenuating antimicrobial resistance. *Nanomaterials* **2022**, *12*, 1115. [[CrossRef](#)]
21. Iqbal, M.S.; Abbas, K.; Qadir, M.I. Synthesis, characterization and evaluation of biological properties of selenium nanoparticles from *Solanum lycopersicum*. *Arab. J. Chem.* **2022**, *15*, 103901.
22. Tyagi, P.K.; Tyagi, S.; Gola, D.; Arya, A.; Ayatollahi, S.A.; Alshehri, M.M.; Sharifi-Rad, J. Ascorbic acid and polyphenols mediated green synthesis of silver nanoparticles from *Tagetes erecta* L. aqueous leaf extract and studied their antioxidant properties. *J. Nanomater.* **2021**, *2021*, 6515419. [[CrossRef](#)]
23. Das, G.; Patra, J.K.; Debnath, T.; Ansari, A.; Shin, H.-S. Investigation of antioxidant, antibacterial, antidiabetic, and cytotoxicity potential of silver nanoparticles synthesized using the outer peel extract of *Ananas comosus* (L.). *PLoS ONE* **2019**, *14*, e0220950. [[CrossRef](#)] [[PubMed](#)]
24. Nasrollahzadeh, M.; Mahmoudi-Gom Yek, S.; Motahharifar, N.; Ghafori Gorab, M.J. Recent developments in the plant-mediated green synthesis of Ag-based nanoparticles for environmental and catalytic applications. *Chem. Rec.* **2019**, *19*, 2436–2479. [[CrossRef](#)] [[PubMed](#)]
25. Qamer, S.; Romli, M.H.; Che-Hamzah, F.; Misni, N.; Joseph, N.M.; Al-Haj, N.A.; Amin-Nordin, S. Systematic review on biosynthesis of silver nanoparticles and antibacterial activities: Application and theoretical perspectives. *Molecules* **2021**, *26*, 5057. [[CrossRef](#)] [[PubMed](#)]
26. Yang, S.-Z.; Liu, Q.-A.; Liu, Y.-L.; Weng, G.-J.; Zhu, J.; Li, J.-J. Recent progress in the optical detection of pathogenic bacteria based on noble metal nanoparticles. *Microchim. Acta* **2021**, *188*, 258. [[CrossRef](#)] [[PubMed](#)]
27. Kowalczyk, P.; Szymczak, M.; Maciejewska, M.; Laskowski, Ł.; Laskowska, M.; Ostaszewski, R.; Skiba, G.; Franiak-Pietryga, I.J. All that glitters is not silver—A new look at microbiological and medical applications of silver nanoparticles. *Int. J. Mol. Sci.* **2021**, *22*, 854. [[CrossRef](#)]
28. Kukushkina, E.A.; Hossain, S.I.; Sportelli, M.C.; Ditaranto, N.; Picca, R.A.; Cioffi, N.J. Ag-based synergistic antimicrobial composites. A critical review. *Nanomaterials* **2021**, *11*, 1687. [[CrossRef](#)]
29. Crisan, C.M.; Mocan, T.; Manolea, M.; Lasca, L.I.; Tăbăran, F.-A.; Mocan, L.J. Review on silver nanoparticles as a novel class of antibacterial solutions. *Appl. Sci.* **2021**, *11*, 1120. [[CrossRef](#)]
30. Kaiser, K.G.; Delattre, V.; Frost, V.J.; Buck, G.W.; Phu, J.V.; Fernandez, T.G.; Pavel, I.E. Nanosilver: An old antibacterial agent with great promise in the fight against antibiotic resistance. *Antibiotics* **2023**, *12*, 1264. [[CrossRef](#)]

31. Chinemerem Nwobodo, D.; Ugwu, M.C.; Oliseloke Anie, C.; Al-Ouqaili, M.T.; Chinedu Ikem, J.; Victor Chigozie, U.; Saki, M.J. Antibiotic resistance: The challenges and some emerging strategies for tackling a global menace. *J. Clin. Lab. Anal.* **2022**, *36*, e24655. [[CrossRef](#)]
32. Szerencsés, B.; Igaz, N.; Tóbiás, Á.; Prucsi, Z.; Rónavári, A.; Béteky, P.; Madarász, D.; Papp, C.; Makra, I.; Vágvölgyi, C. Size-dependent activity of silver nanoparticles on the morphological switch and biofilm formation of opportunistic pathogenic yeasts. *BMC Microbiol.* **2020**, *20*, 176. [[CrossRef](#)] [[PubMed](#)]
33. Alsamman, A.M.; Khedr, M.; Kabary, H.A.; El-Sehrawy, M. Elimination of pathogenic multidrug resistant isolates through different metal oxide nanoparticles synthesized from organic plant and microbial sources. *Microb. Pathog.* **2023**, *178*, 106055. [[CrossRef](#)] [[PubMed](#)]
34. Oves, M.; Rauf, M.A.; Aslam, M.; Qari, H.A.; Sonbol, H.; Ahmad, I.; Zaman, G.S.; Saeed, M. Green synthesis of silver nanoparticles by *Conocarpus lancifolius* plant extract and their antimicrobial and anticancer activities. *Saudi J. Biol. Sci.* **2022**, *29*, 460–471. [[CrossRef](#)]
35. Fouda, A.; Awad, M.A.; Eid, A.M.; Saied, E.; Barghoth, M.G.; Hamza, M.F.; Awad, M.F.; Abdelbary, S.; Hassan, S.E.-D. An eco-friendly approach to the control of pathogenic microbes and *Anopheles stephensi* malarial vector using magnesium oxide nanoparticles (Mg-nps) fabricated by *Penicillium chrysogenum*. *Int. J. Mol. Sci.* **2021**, *22*, 5096. [[CrossRef](#)]
36. Ondari, D.M. Urinary Tract Infections Caused by Enteric Bacteria and Antibiotic Sensitivity among Symptomatic Males Visiting Special Treatment Center. Master's Thesis, Kenyatta University, Nairobi, Kenya, 2020.
37. Thijs, S.; Op De Beeck, M.; Beckers, B.; Truyens, S.; Stevens, V.; Van Hamme, J.D.; Weyens, N.; Vangronsveld, J. Comparative evaluation of four bacteria-specific primer pairs for 16S rRNA gene surveys. *Front. Microbiol.* **2017**, *8*, 494. [[CrossRef](#)] [[PubMed](#)]
38. Green, M.R.; Sambrook, J. Analysis of DNA by agarose gel electrophoresis. *Cold Spring Harb. Protoc.* **2019**, 2019, pdb.top100388. [[CrossRef](#)]
39. Mekky, A.E.; Emam, A.E.; Selim, M.N.; Abdelmouty, E.S.; Khedr, M. Antibacterial and antineoplastic MCF-7 and HePG-2 characteristics of the methanolic (80%) clove (*Syzygium aromaticum* L.) extract. *Biorefinery* **2023**, *2023*, 1–12. [[CrossRef](#)]
40. Kenia, P.N. Effect of Catecholamines and Inhaled Drugs on the Growth and Virulence of Bacterial Respiratory Pathogens. Doctoral Dissertation, University of Leicester, Leicester, UK, 2019.
41. Feizi, S.; Taghipour, E.; Ghadam, P.; Mohammadi, P. Antifungal, antibacterial, antibiofilm and colorimetric sensing of toxic metals activities of eco friendly, economical synthesized Ag/AgCl nanoparticles using *Malva sylvestris* leaf extracts. *Microb. Pathog.* **2018**, *125*, 33–42. [[CrossRef](#)]
42. Hashem, A.H.; Saied, E.; Amin, B.H.; Alotibi, F.O.; Al-Askar, A.A.; Arishi, A.A.; Elkady, F.M.; Elbahnasawy, M.A. Antifungal activity of biosynthesized silver nanoparticles (AgNPs) against aspergilli causing aspergillosis: Ultrastructure Study. *J. Funct. Biomater.* **2022**, *13*, 242. [[CrossRef](#)]
43. Bhakya, S.; Muthukrishnan, S.; Sukumaran, M.; Muthukumar, M. Biogenic synthesis of silver nanoparticles and their antioxidant and antibacterial activity. *Appl. Nanosci.* **2016**, *6*, 755–766. [[CrossRef](#)]
44. Olasunkanmi, A.A.; Afuye, O. Evaluation of In Vitro Anti-Inflammatory Potential of Aqueous Solanum Aethiopicum (Garden Egg) Leaf Extract. *Furth. Biomed.* **2021**, *1*, 1–14.
45. Sofowora, A. *Medicinal Plants and Traditional Medicine in Africa. Nigeria*; Spectrum Book Ltd.: New Delhi, India, 1993; pp. 195–238.
46. Mojab, F.; Kamalnehad, M.; Ghaderi, N.; Vahidi, P.H. Phytochemical screening of some species of Iranian plants. *Iran. J. Pharm. Res. IJPR* **2003**, *2*, 77–82.
47. Evans, W. *Trease and Evans Pharmacognosy*, 15th ed.; Saunders Publishers: New Delhi, India, 2002.
48. Salna, K.; Sreejith, K.; Uthiralingam, M.; Mithu, A.P.; John Milton, M.; Albin, T.F. A comparative study of phytochemicals investigation of *Andrographis paniculata* and *Murraya koenigii*. *Int. J. Pharm. Pharm. Sci.* **2011**, *3*, 291–292.
49. Preshant, T.; Bimlesh, K.; Mandeep, K.; Gurpreet, K.; Harleen, K. Phytochemical screening and extraction: A review. *Int. Pharm. Sci.* **2011**, *1*, 98–108.
50. Harsha, N.; Sridevi, V.; Lakshmi, M.; Rani, K.; Vani, N.D.S. Phytochemical analysis of some selected spices. *Int. J. Innov. Res. Sci. Eng. Technol.* **2013**, *2*, 6618–6621.
51. Balbaa, S. *Chemistry of Crude Drugs*; Cairo University: Cairo, Egypt, 1986; Volume 195.
52. Shaikh, J.R.; Patil, M. Qualitative tests for preliminary phytochemical screening: An overview. *Int. J. Chem. Stud.* **2020**, *8*, 603–608. [[CrossRef](#)]
53. Farooq, Z.; Al Naqqash, Z.A.; Eldalawy, R. Phytochemical screening, GC/MS analysis and antibacterial activity of *Coriandrum sativum* L. seed. *Res. J. Pharm. Technol.* **2022**, *15*, 4033–4036. [[CrossRef](#)]
54. Abdullahi, D.; Michael, O.; Indabawa, I.I. Antibacterial activities and phytochemical screening of aloe vera (*A. babardensis*), garlic (*A sativum*) and ginger (*Z officinale*). *J. Emerg. Trends Eng. Appl. Sci.* **2014**, *5*, 172–178.
55. Egbuna, C.; Ifemeje, J.C.; Maduako, M.C.; Tijjani, H.; Udedi, S.C.; Nwaka, A.C.; Ifemeje, M.O. Phytochemical test methods: Qualitative, quantitative and proximate analysis. *Phytochemistry* **2018**, *1*, 381–425.
56. Kebede, T.; Gadisa, E.; Tufa, A. Antimicrobial activities evaluation and phytochemical screening of some selected medicinal plants: A possible alternative in the treatment of multidrug-resistant microbes. *PLoS ONE* **2021**, *16*, e0249253. [[CrossRef](#)] [[PubMed](#)]
57. Makkar, H.P. *Quantification of Tannins in Tree and Shrub Foliage: A Laboratory Manual*; Springer Science & Business Media: Berlin/Heidelberg, Germany, 2003.
58. Savych, A.; Milian, I. Total flavonoid content in the herbal mixture with antidiabetic activity. *PharmacologyOnLine* **2021**, *2*, 68–75.

59. Martins, G.R.; Monteiro, A.F.; do Amaral, F.R.L.; da Silva, A.S.A. A validated Folin-Ciocalteu method for total phenolics quantification of condensed tannin-rich açai (*Euterpe oleracea* Mart.) seeds extract. *J. Food Sci. Technol.* **2021**, *58*, 4693–4702. [CrossRef] [PubMed]
60. Lim, J.G.; Park, H.M.; Yoon, K.S. Analysis of saponin composition and comparison of the antioxidant activity of various parts of the quinoa plant (*Chenopodium quinoa* Willd.). *Food Sci. Nutr.* **2020**, *8*, 694–702. [CrossRef] [PubMed]
61. Harborne, A. *Phytochemical Methods a Guide to Modern Techniques of Plant Analysis*; Springer Science & Business Media: Berlin/Heidelberg, Germany, 1998.
62. Saber, H.; Alwaleed, E.A.; Ebnalwaled, K.; Sayed, A.; Salem, W. Efficacy of silver nanoparticles mediated by *Jania rubens* and *Sargassum dentifolium* macroalgae; Characterization and biomedical applications. *Egypt. J. Basic Appl. Sci.* **2017**, *4*, 249–255. [CrossRef]
63. White, T.J.; Bruns, T.; Lee, S.; Taylor, J. Amplification and direct sequencing of fungal ribosomal RNA genes for phylogenetics. *PCR Protoc. A Guide Methods Appl.* **1990**, *18*, 315–322.
64. Saied, E.; Hussein, A.S.; Al-Askar, A.A.; Elhussieny, N.I.; Hashem, A.H. Therapeutic effect of biosynthesized silver nanoparticles on hypothyroidism induced in albino rats. *Electron. J. Biotechnol.* **2023**, *65*, 14–23. [CrossRef]
65. Sarkar, J.; Naskar, A.; Nath, A.; Gangopadhyay, B.; Tarafdar, E.; Das, D.; Chakraborty, S.; Chattopadhyay, D.; Acharya, K. Innovative utilization of harvested mushroom substrate for green synthesis of silver nanoparticles: A Multi-Response optimization approach. *Environ. Res.* **2024**, 118297. [CrossRef]
66. Chinnaiyah, K.; Krishnamoorthi, R.; Kannan, K.; Sivaganesh, D.; Saravanakumar, S.; Theivasanthi, T.; Palko, N.; Grishina, M.; Maik, V.; Gurushankar, K. Ag nanoparticles synthesized by *Datura metel* L. Leaf extract and their charge density distribution, electrochemical and biological performance. *Chem. Phys. Lett.* **2022**, *807*, 140083. [CrossRef]
67. Iram, F.; Yasmeen, A.; Massey, S.; Iqbal, M.S.; Asim, S.; Irshad, M.; Zahid, H.; Khan, A.Y.; Kazimi, S.G. Synthesis of gold and silver nanoparticles by use of arabinoglucan from *Lallemantia royleana*. *Int. J. Biol. Macromol.* **2021**, *191*, 1137–1150. [CrossRef]
68. Saied, E.; Hashem, A.H.; Ali, O.M.; Selim, S.; Almuhayawi, M.S.; Elbahnasawy, M.A. Photocatalytic and antimicrobial activities of biosynthesized silver nanoparticles using *Cytobacillus firmus*. *Life* **2022**, *12*, 1331. [CrossRef] [PubMed]
69. Adeyemi, O.S.; Uloko, R.A.; Awakan, O.J.; Adeyanju, A.A.; Otohinoiyi, D.A. The oral administration of silver nanoparticles activates the kynurenine pathway in rat brain independently of oxidative stress. *Chem. Interact.* **2019**, *302*, 22–27. [CrossRef] [PubMed]
70. Adeyemi, O.S.; Shittu, E.O.; Akpor, O.B.; Rotimi, D.; Batiha, G.E. Silver nanoparticles restrict microbial growth by promoting oxidative stress and DNA damage. *EXCLI J.* **2020**, *19*, 492. [PubMed]
71. Hosnedlova, B.; Kabanov, D.; Kepinska, M.; Narayanan, V.H.B.; Parikesit, A.A.; Fernandez, C.; Bjørklund, G.; Nguyen, H.V.; Farid, A.; Sochor, J. Effect of Biosynthesized Silver Nanoparticles on Bacterial Biofilm Changes in *S. aureus* and *E. coli*. *Nanomaterials* **2022**, *12*, 2183. [CrossRef] [PubMed]
72. de Lacerda Coriolano, D.; de Souza, J.B.; Bueno, E.V.; Medeiros, S.M.d.F.R.d.S.; Cavalcanti, I.D.L.; Cavalcanti, I.M.F. Antibacterial and antibiofilm potential of silver nanoparticles against antibiotic-sensitive and multidrug-resistant *Pseudomonas aeruginosa* strains. *Braz. J. Microbiol.* **2021**, *52*, 267–278. [CrossRef] [PubMed]
73. Soni, V.; Raizada, P.; Singh, P.; Cuong, H.N.; Rangabhashiyam, S.; Saini, A.; Saini, R.V.; Van Le, Q.; Nadda, A.K.; Le, T.-T. Sustainable and green trends in using plant extracts for the synthesis of biogenic metal nanoparticles toward environmental and pharmaceutical advances: A review. *Environ. Res.* **2021**, *202*, 111622. [CrossRef]
74. Bandeira, M.; Giovanela, M.; Roesch-Ely, M.; Devine, D.M.; da Silva Crespo, J. Green synthesis of zinc oxide nanoparticles: A review of the synthesis methodology and mechanism of formation. *Sustain. Chem. Pharm.* **2020**, *15*, 100223. [CrossRef]
75. Shamaila, S.; Sajjad, A.K.L.; Farooqi, S.A.; Jabeen, N.; Majeed, S.; Farooq, I. Advancements in nanoparticle fabrication by hazard free eco-friendly green routes. *Appl. Mater. Today* **2016**, *5*, 150–199. [CrossRef]
76. Singh, J.; Dutta, T.; Kim, K.-H.; Rawat, M.; Samddar, P.; Kumar, P. 'Green' synthesis of metals and their oxide nanoparticles: Applications for environmental remediation. *J. Nanobiotechnol.* **2018**, *16*, 84. [CrossRef]
77. Dikshit, P.K.; Kumar, J.; Das, A.K.; Sadhu, S.; Sharma, S.; Singh, S.; Gupta, P.K.; Kim, B.S. Green synthesis of metallic nanoparticles: Applications and limitations. *Catalysts* **2021**, *11*, 902. [CrossRef]
78. Al-Askar, A.A.; Hashem, A.H.; Elhussieny, N.I.; Saied, E. Green Biosynthesis of Zinc Oxide Nanoparticles Using *Pluchea indica* Leaf Extract: Antimicrobial and Photocatalytic Activities. *Molecules* **2023**, *28*, 4679. [CrossRef] [PubMed]
79. Mostafa, Y.S.; Alamri, S.A.; Alrumman, S.A.; Hashem, M.; Baka, Z.A. Green synthesis of silver nanoparticles using pomegranate and orange peel extracts and their antifungal activity against *Alternaria solani*, the causal agent of early blight disease of tomato. *Plants* **2021**, *10*, 2363. [CrossRef] [PubMed]
80. Ali, E.; Abd-Elhalim, B.T.; Hesham, E.; Ahmed, S.; Mostafa, H.; Gamal, A.; El-Sayed, S.M.; Hemdan, B.; Bakry, A.; Ebeed, N.; et al. Eco-Friendly Biosynthesis and Characterization of Silver Nanoparticles from *Solanum lycopersicum* (Tomato) Peel Waste and Its Application in Disinfecting Metallic Surfaces. 2023. Available online: <https://www.researchsquare.com/article/rs-3100232/v1> (accessed on 6 July 2023).
81. Singh, R.; Hano, C.; Nath, G.; Sharma, B. Green biosynthesis of silver nanoparticles using leaf extract of *Carissa carandas* L. and their antioxidant and antimicrobial activity against human pathogenic bacteria. *Biomolecules* **2021**, *11*, 299. [CrossRef]

82. Bharathi, D.; Preethi, S.; Abarna, K.; Nithyasri, M.; Kishore, P.; Deepika, K.J.B.; Biotechnology, A. Bio-inspired synthesis of flower shaped iron oxide nanoparticles (FeONPs) using phytochemicals of *Solanum lycopersicum* leaf extract for biomedical applications. *Biocatal. Agric. Biotechnol.* **2020**, *27*, 101698. [[CrossRef](#)]
83. Elbrolesy, A.; Abdou, Y.; Elhussiny, F.; Morsy, R. Novel Green Synthesis of UV-Sunscreen ZnO Nanoparticles Using *Solanum lycopersicum* Fruit Extract and Evaluation of Their Antibacterial and Anticancer Activity. *J. Inorg. Organomet. Polym. Mater.* **2023**, *33*, 3750–3759. [[CrossRef](#)]
84. Rodríguez-Varillas, S.; Fontanil, T.; Obaya, Á.J.; Fernández-González, A.; Murru, C.; Badía-Laiño, R. Biocompatibility and antioxidant capabilities of carbon dots obtained from tomato (*Solanum lycopersicum*). *Appl. Sci.* **2022**, *12*, 773. [[CrossRef](#)]
85. Alsharif, S.M.; Salem, S.S.; Abdel-Rahman, M.A.; Fouda, A.; Eid, A.M.; Hassan, S.E.-D.; Awad, M.A.; Mohamed, A.A. Multifunctional properties of spherical silver nanoparticles fabricated by different microbial taxa. *Heliyon* **2020**, *6*, e03943. [[CrossRef](#)]
86. Nallal, V.U.M.; Prabha, K.; VethaPotheher, I.; Ravindran, B.; Baazeem, A.; Chang, S.W.; Otunola, G.A.; Razia, M. Sunlight-driven rapid and facile synthesis of Silver nanoparticles using *Allium ampeloprasum* extract with enhanced antioxidant and antifungal activity. *Saudi J. Biol. Sci.* **2021**, *28*, 3660–3668. [[CrossRef](#)]
87. Elgendy, M.Y.; Shaalan, M.; Abdelsalam, M.; Eissa, A.E.; El-Adawy, M.M.; Seida, A.A. Antibacterial activity of silver nanoparticles against antibiotic-resistant *Aeromonas veronii* infections in *Nile tilapia*, *Oreochromis niloticus* (L.), in vitro and in vivo assay. *Aquac. Res.* **2022**, *53*, 901–920. [[CrossRef](#)]
88. El-Bendary, M.A.; Moharam, M.E.; Hamed, S.R.; Abo El-Ola, S.M.; Khalil, S.K.; Mounier, M.M.; Roshdy, A.M.; Allam, M.A. Mycosynthesis of silver nanoparticles using *Aspergillus caespitosus*: Characterization, antimicrobial activities, cytotoxicity, and their performance as an antimicrobial agent for textile materials. *Appl. Organomet. Chem.* **2021**, *35*, e6338. [[CrossRef](#)]
89. Pallavi, S.; Rudayni, H.A.; Bepari, A.; Niazi, S.K.; Nayaka, S. Green synthesis of Silver nanoparticles using *Streptomyces hirsutus* strain SNPGA-8 and their characterization, antimicrobial activity, and anticancer activity against human lung carcinoma cell line A549. *Saudi J. Biol. Sci.* **2022**, *29*, 228–238.
90. Sudarsan, S.; Kumar Shankar, M.; Kumar Belagal Motatis, A.; Shankar, S.; Krishnappa, D.; Mohan, C.D.; Rangappa, K.S.; Gupta, V.K.; Siddaiah, C.N. Green synthesis of silver nanoparticles by *Cytobacillus firmus* isolated from the stem bark of *Terminalia arjuna* and their antimicrobial activity. *Biomolecules* **2021**, *11*, 259. [[CrossRef](#)] [[PubMed](#)]
91. Elshafei, A.M.; Othman, A.M.; Elsayed, M.A.; Al-Balakocy, N.G.; Hassan, M.M. Green synthesis of silver nanoparticles using *Aspergillus oryzae* NRRL447 exogenous proteins: Optimization via central composite design, characterization and biological applications. *Environ. Nanotechnol. Monit. Manag.* **2021**, *16*, 100553. [[CrossRef](#)]
92. Khanal, L.N.; Sharma, K.R.; Paudyal, H.; Parajuli, K.; Dahal, B.; Ganga, G.; Pokharel, Y.R.; Kalauni, S.K. Green synthesis of silver nanoparticles from root extracts of *Rubus ellipticus* Sm. and comparison of antioxidant and antibacterial activity. *J. Nanomater.* **2022**, *2022*, 1832587. [[CrossRef](#)]
93. El-Gamal, M.S.; Salem, S.S.; Abdo, A.M. Biosynthesis, characterization, and antimicrobial activities of silver nanoparticles synthesized by endophytic *Streptomyces* sp. *J. Biotechnol.* **2018**, *56*, 69–85.
94. Ajitha, B.; Reddy, Y.A.K.; Lee, Y.; Kim, M.J.; Ahn, C.W. Biomimetic synthesis of silver nanoparticles using *Syzygium aromaticum* (clove) extract: Catalytic and antimicrobial effects. *Appl. Organomet. Chem.* **2019**, *33*, e4867. [[CrossRef](#)]
95. Chi, N.T.L.; Veeraragavan, G.R.; Brindhadevi, K.; Chinnathambi, A.; Salmen, S.H.; Alharbi, S.A.; Krishnan, R.; Pugazhendhi, A. Fungi fabrication, characterization, and anticancer activity of silver nanoparticles using metals resistant *Aspergillus niger*. *Environ. Res.* **2022**, *208*, 112721.
96. Khorrami, S.; Zarrabi, A.; Khaleghi, M.; Danaei, M.; Mozafari, M. Selective cytotoxicity of green synthesized silver nanoparticles against the MCF-7 tumor cell line and their enhanced antioxidant and antimicrobial properties. *Int. J. Nanomed.* **2018**, *13*, 8013–8024. [[CrossRef](#)]
97. Nagaraja, S.K.; Niazi, S.K.; Bepari, A.; Assiri, R.A.; Nayaka, S. Leonotis nepetifolia flower bud extract mediated green synthesis of silver nanoparticles, their characterization, and in vitro evaluation of biological applications. *Materials* **2022**, *15*, 8990. [[CrossRef](#)]
98. Hamouda, R.A.; Hussein, M.H.; Abo-Elmagd, R.A.; Bawazir, S.S. Synthesis and biological characterization of silver nanoparticles derived from the cyanobacterium *Oscillatoria limnetica*. *Sci. Rep.* **2019**, *9*, 13071. [[CrossRef](#)]
99. Lakhan, M.N.; Chen, R.; Shar, A.H.; Chand, K.; Shah, A.H.; Ahmed, M.; Ali, I.; Ahmed, R.; Liu, J.; Takahashi, K. Eco-friendly green synthesis of clove buds extract functionalized silver nanoparticles and evaluation of antibacterial and antidiatom activity. *J. Microbiol. Methods* **2020**, *173*, 105934. [[CrossRef](#)] [[PubMed](#)]
100. Hemlata; Meena, P.R.; Singh, A.P.; Tejavath, K.K. Biosynthesis of silver nanoparticles using *Cucumis prophetarum* aqueous leaf extract and their antibacterial and antiproliferative activity against cancer cell lines. *ACS Omega* **2020**, *5*, 5520–5528. [[CrossRef](#)] [[PubMed](#)]
101. Küp, F.Ö.; Çoşkunçay, S.; Duman, F. Biosynthesis of silver nanoparticles using leaf extract of *Aesculus hippocastanum* (horse chestnut): Evaluation of their antibacterial, antioxidant and drug release system activities. *Mater. Sci. Eng. C* **2020**, *107*, 110207. [[CrossRef](#)] [[PubMed](#)]
102. Manik, U.; Nande, A.; Raut, S.; Dhoble, S. Green synthesis of silver nanoparticles using plant leaf extraction of *Artocarpus heterophyllus* and *Azadirachta indica*. *Results Mater.* **2020**, *6*, 100086. [[CrossRef](#)]
103. Rajkumar, P.; Prakasam, A.; Rajeshkumar, S.; Gomathi, M.; Anbarasan, P.; Chandrasekaran, R. Green synthesis of silver nanoparticles using *Gynemna sylvestre* leaf extract and evaluation of its antibacterial activity. *S. Afr. J. Chem. Eng.* **2020**, *32*, 1–4.

104. Abdelrazik, M.; Elkotaby, H.H.; Yousef, A.; El-Sayed, A.F.; Khedr, M. Green synthesis of silver nanoparticles derived from lemon and pomegranate peel extracts to combat multidrug-resistant bacterial isolates. *J. Genet. Eng. Biotechnol.* **2023**, *21*, 97. [[CrossRef](#)] [[PubMed](#)]
105. Khedr, M.; Youssef, F.S.; El-Kattan, N.; Abozahra, M.S.; Selim, M.N.; Yousef, A.; Khalil, K.M.; Mekky, A.E. FolE gene expression for folic acid productivity from optimized and characterized probiotic *Lactobacillus delbrueckii*. *J. Genet. Eng. Biotechnol.* **2023**, *21*, 169. [[CrossRef](#)] [[PubMed](#)]
106. Di Meo, S.; Venditti, P.J.O.M.; Longevity, C. Evolution of the knowledge of free radicals and other oxidants. *Oxidative Med. Cell. Longev.* **2020**, *2020*, 9829176. [[CrossRef](#)]
107. Kumar, H.; Bhardwaj, K.; Nepovimova, E.; Kuča, K.; Singh Dhanjal, D.; Bhardwaj, S.; Bhatia, S.K.; Verma, R.; Kumar, D. Antioxidant functionalized nanoparticles: A combat against oxidative stress. *Nanomaterials* **2020**, *10*, 1334. [[CrossRef](#)]
108. Shehabeldine, A.M.; Salem, S.S.; Ali, O.M.; Abd-Elsalam, K.A.; Elkady, F.M.; Hashem, A.H. Multifunctional silver nanoparticles based on chitosan: Antibacterial, antibiofilm, antifungal, antioxidant, and wound-healing activities. *J. Fungi* **2022**, *8*, 612. [[CrossRef](#)]
109. Rajivgandhi, G.N.; Ramachandran, G.; Maruthupandy, M.; Manoharan, N.; Alharbi, N.S.; Kadaikunnan, S.; Khaled, J.M.; Almanaa, T.N.; Li, W.-J.J.C.; Physicochemical, S.A.; et al. Anti-oxidant, anti-bacterial and anti-biofilm activity of biosynthesized silver nanoparticles using *Gracilaria corticata* against biofilm producing *K. pneumoniae*. *Colloids Surf. A Physicochem. Eng. Asp.* **2020**, *600*, 124830. [[CrossRef](#)]
110. Gambogou, B.; Taale, E.; Anani, K.; Kangni-Dossou, M.; Karou, D.S.; Ameyapoh, Y. Microbiological analysis and assessment of the Biotechnological potential of *Lactobacillus* sp. and *Pediococcus* sp. strains isolated from Togolese traditional Zea mays fermented food. *J. Food Sci. Nutr. Res.* **2023**, *6*, 155–164. [[CrossRef](#)]
111. Dridi, R.; Essghaier, B.; Hannachi, H.; Khedher, G.B.; Chaffei, C.; Zid, M.F. Biosynthesized silver nanoparticles using *Anagallis monelli*: Evaluation of antioxidant activity, antibacterial and antifungal effects. *J. Mol. Struct.* **2022**, *1251*, 132076. [[CrossRef](#)]
112. Rajeshkumar, S.; Kumar, S.V.; Ramaiah, A.; Agarwal, H.; Lakshmi, T.; Roopan, S.M. Biosynthesis of zinc oxide nanoparticles using *Mangifera indica* leaves and evaluation of their antioxidant and cytotoxic properties in lung cancer (A549) cells. *Enzym. Microb. Technol.* **2018**, *117*, 91–95. [[CrossRef](#)] [[PubMed](#)]
113. Govindappa, M.; Tejashree, S.; Thanuja, V.; Hemashekhar, B.; Srinivas, C.; Nasif, O.; Pugazhendhi, A.; Raghavendra, V.B. Pomegranate fruit fleshy pericarp mediated silver nanoparticles possessing antimicrobial, antibiofilm formation, antioxidant, biocompatibility and anticancer activity. *J. Drug Deliv. Sci. Technol.* **2021**, *61*, 102289. [[CrossRef](#)]
114. Talank, N.; Morad, H.; Barabadi, H.; Mojab, F.; Amidi, S.; Kobarfard, F.; Mahjoub, M.A.; Jounaki, K.; Mohammadi, N.; Salehi, G. Bioengineering of green-synthesized silver nanoparticles: In vitro physicochemical, antibacterial, biofilm inhibitory, anticoagulant, and antioxidant performance. *Talanta* **2022**, *243*, 123374. [[CrossRef](#)] [[PubMed](#)]
115. Kumar, V.; Singh, S.; Srivastava, B.; Bhadouria, R.; Singh, R. Green synthesis of silver nanoparticles using leaf extract of *Holoptelea integrifolia* and preliminary investigation of its antioxidant, anti-inflammatory, antidiabetic and antibacterial activities. *J. Environ. Chem. Eng.* **2019**, *7*, 103094. [[CrossRef](#)]
116. Zaki, A.; Aziz, M.N.; Ahmad, R.; Ahamad, I.; Ali, M.S.; Yasin, D.; Afzal, B.; Ali, S.M.; Chopra, A.; Hadda, V. Synthesis, purification and characterization of Plectonema derived AgNPs with elucidation of the role of protein in nanoparticle stabilization. *RSC Adv.* **2022**, *12*, 2497–2510. [[CrossRef](#)]
117. ASTM F756-00; Standard Practice for Assessment of Hemolytic Properties of Materials. ASTM International: Conshohocken, PA, USA, 2000.
118. Hajji, S.; Khedir, S.B.; Hamza-Mnif, I.; Hamdi, M.; Jedidi, I.; Kallel, R.; Boufi, S.; Nasri, M. Biomedical potential of chitosan-silver nanoparticles with special reference to antioxidant, antibacterial, hemolytic and in vivo cutaneous wound healing effects. *Biochim. Biophys. Acta BBA-Gen. Subj.* **2019**, *1863*, 241–254. [[CrossRef](#)]
119. Chahardoli, A.; Hajmomeni, P.; Ghowsi, M.; Qalekhani, F.; Shokoohinia, Y.; Fattahi, A. Optimization of quercetin-assisted silver nanoparticles synthesis and evaluation of their hemocompatibility, antioxidant, anti-inflammatory, and antibacterial effects. *Glob. Chall.* **2021**, *5*, 2100075. [[CrossRef](#)]
120. Sharifi-Rad, M.; Pohl, P.; Epifano, F.; Álvarez-Suarez, J.M. Green synthesis of silver nanoparticles using *Astragalus tribuloides* delile. root extract: Characterization, antioxidant, antibacterial, and anti-inflammatory activities. *Nanomaterials* **2020**, *10*, 2383. [[CrossRef](#)] [[PubMed](#)]
121. Sabarathinam, J.; Madhulaxmi, R. Development of anti inflammatory and antimicrobial silver nanoparticles coated suture materials. *Int. J. Dent. Oral Sci.* **2021**, *8*, 2006–2013.
122. Marahatha, R.; Gyawali, K.; Sharma, K.; Gyawali, N.; Tandan, P.; Adhikari, A.; Timilsina, G.; Bhattarai, S.; Lamichhane, G.; Acharya, A. Pharmacologic activities of phytosteroids in inflammatory diseases: Mechanism of action and therapeutic potentials. *Phytother. Res.* **2021**, *35*, 5103–5124. [[CrossRef](#)]
123. Salve, P.; Vinchurkar, A.; Raut, R.; Chondekar, R.; Lakkakula, J.; Roy, A.; Hossain, M.J.; Alghamdi, S.; Almeahmadi, M.; Abdulaziz, O. An evaluation of antimicrobial, anticancer, anti-inflammatory and antioxidant activities of silver nanoparticles synthesized from leaf extract of *Madhuca longifolia* utilizing quantitative and qualitative methods. *Molecules* **2022**, *27*, 6404. [[CrossRef](#)] [[PubMed](#)]

124. Nagime, P.V.; Singh, S.; Shaikh, N.M.; Gomare, K.S.; Chitme, H.; Abdel-Wahab, B.A.; Alqahtany, Y.S.; Khateeb, M.M.; Habeeb, M.S.; Bakir, M.B. Biogenic Fabrication of Silver Nanoparticles Using *Calotropis procera* Flower Extract with Enhanced Biomimetics Attributes. *Materials* **2023**, *16*, 4058. [[CrossRef](#)] [[PubMed](#)]
125. Zhao, Q.; Zhu, L.; Wang, S.; Gao, Y.; Jin, F. Molecular mechanism of the anti-inflammatory effects of plant essential oils: A systematic review. *J. Ethnopharmacol.* **2023**, *301*, 115829. [[CrossRef](#)] [[PubMed](#)]
126. Laurindo, L.F.; de Carvalho, G.M.; de Oliveira Zanuso, B.; Figueira, M.E.; Direito, R.; de Alvares Goulart, R.; Buglio, D.S.; Barbalho, S.M. Curcumin-Based Nanomedicines in the Treatment of Inflammatory and Immunomodulated Diseases: An Evidence-Based Comprehensive Review. *Pharmaceutics* **2023**, *15*, 229. [[CrossRef](#)]
127. Chi, N.T.L.; Narayanan, M.; Chinnathambi, A.; Govindasamy, C.; Subramani, B.; Brindhadevi, K.; Pimpimon, T.; Pikulkaew, S. Fabrication, characterization, anti-inflammatory, and anti-diabetic activity of silver nanoparticles synthesized from *Azadirachta indica* kernel aqueous extract. *Environ. Res.* **2022**, *208*, 112684.
128. Gajdács, M.; Ábrók, M.; Lázár, A.; Burián, K. Increasing relevance of Gram-positive cocci in urinary tract infections: A 10-year analysis of their prevalence and resistance trends. *Sci. Rep.* **2020**, *10*, 17658. [[CrossRef](#)]
129. Stefaniuk, E.; Suchocka, U.; Bosacka, K.; Hryniewicz, W. Etiology and antibiotic susceptibility of bacterial pathogens responsible for community-acquired urinary tract infections in Poland. *Eur. J. Clin. Microbiol. Infect. Dis.* **2016**, *35*, 1363–1369. [[CrossRef](#)]
130. Flores-Mireles, A.L.; Walker, J.N.; Caparon, M.; Hultgren, S.J. Urinary tract infections: Epidemiology, mechanisms of infection and treatment options. *Nat. Rev. Microbiol.* **2015**, *13*, 269–284. [[CrossRef](#)] [[PubMed](#)]
131. Loo, Y.Y.; Rukayadi, Y.; Nor-Khaizura, M.-A.-R.; Kuan, C.H.; Chieng, B.W.; Nishibuchi, M.; Radu, S. In vitro antimicrobial activity of green synthesized silver nanoparticles against selected gram-negative foodborne pathogens. *Front. Microbiol.* **2018**, *9*, 1555. [[CrossRef](#)] [[PubMed](#)]
132. Khaydarov, R.R.; Khaydarov, R.A.; Evgrafova, S.; Wagner, S.; Cho, S.Y. Environmental and human health issues of silver nanoparticles applications. In *Environmental Security and Ecoterrorism*; Springer: Dordrecht, The Netherlands, 2011; pp. 117–127.
133. Yousef, A.; Abu-Elghait, M.; Barghoth, M.G.; Elazzazy, A.M.; Desouky, S.E. Fighting multidrug-resistant *Enterococcus faecalis* via interfering with virulence factors using green synthesized nanoparticles. *Microb. Pathog.* **2022**, *173*, 105842. [[CrossRef](#)] [[PubMed](#)]
134. Tyavambiza, C.; Elbagory, A.M.; Madiehe, A.M.; Meyer, M.; Meyer, S. The antimicrobial and anti-inflammatory effects of silver nanoparticles synthesised from *Cotyledon orbiculata* aqueous extract. *Nanomaterials* **2021**, *11*, 1343. [[CrossRef](#)] [[PubMed](#)]
135. Yin, I.X.; Zhang, J.; Zhao, I.S.; Mei, M.L.; Li, Q.; Chu, C.H. The antibacterial mechanism of silver nanoparticles and its application in dentistry. *Int. J. Nanomed.* **2020**, *15*, 2555–2562. [[CrossRef](#)] [[PubMed](#)]
136. Paciorek, P.; Żuberek, M.; Grzelak, A. Products of lipid peroxidation as a factor in the toxic effect of silver nanoparticles. *Materials* **2020**, *13*, 2460. [[CrossRef](#)] [[PubMed](#)]
137. More, P.R.; Pandit, S.; Filippis, A.D.; Franci, G.; Mijakovic, I.; Galdiero, M. Silver nanoparticles: Bactericidal and mechanistic approach against drug resistant pathogens. *Microorganisms* **2023**, *11*, 369. [[CrossRef](#)]
138. Abram, S.L.; Fromm, K.M. Handling (nano) silver as antimicrobial agent: Therapeutic window, dissolution dynamics, detection methods and molecular interactions. *Chem.–A Eur. J.* **2020**, *26*, 10948–10971. [[CrossRef](#)]
139. Hamad, A.; Khashan, K.S.; Hadi, A. Silver nanoparticles and silver ions as potential antibacterial agents. *J. Inorg. Organomet. Polym. Mater.* **2020**, *30*, 4811–4828. [[CrossRef](#)]
140. Mohammed, N.; Abdullahi, I.; Bala, S. Preliminary Phytochemical Screening of Healthy and Leaf Curl Virus Infected Tomato (*Solanum lycopersicum*) Leaves. *J. Appl. Sci. Environ. Manag.* **2022**, *26*, 871–876. [[CrossRef](#)]
141. Mehmood, A.; Naveed, K.; Jadoon, N.; Ayub, Q.; Hussain, M.; Hassaan, M. Phytochemical screening and antibacterial efficacy of black cumin (*Nigella sativa* L.) seeds. *FUUAST J. Biol.* **2021**, *11*, 23–28.
142. Mallik, S.; Sharangi, A.; Sarkar, T. Phytochemicals of coriander, cumin, fenugreek, fennel and black cumin: A preliminary study. *Natl. Acad. Sci. Lett.* **2020**, *43*, 477–480. [[CrossRef](#)]
143. Balaram, P.; Vidhya, N.; Rojamathi, K.; Revathi Satheesh, E.; Sowmiya, P.; Sabarish, T.; Mahalingam, P. Antibacterial and Phytochemical Analysis of *Cuminum cyminum* (Cumin) and *Illicium verum* (Star Anise) against Clinical Pathogens. *WJPR* **2021**, *10*, 938–947.

Disclaimer/Publisher’s Note: The statements, opinions and data contained in all publications are solely those of the individual author(s) and contributor(s) and not of MDPI and/or the editor(s). MDPI and/or the editor(s) disclaim responsibility for any injury to people or property resulting from any ideas, methods, instructions or products referred to in the content.